# Data Rate Enhancement in Ultrasonic Data Telemetry Links

Ali Abbasi Shahkooh

A THESIS SUBMITTED TO

THE FACULTY OF GRADUATE STUDIES

IN PARTIAL FULFILLMENT OF THE REQUIREMENTS

FOR THE DEGREE OF

MASTER OF SCIENCE

GRADUATE PROGRAM IN COMPUTER SCIENCE AND ELECTRICAL

ENGINEERING

YORK UNIVERSITY

TORONTO, ONTARIO

April 2022

# Abstract

This research aims at introducing a novel technique for the enhancement of data rate in wireless data transfer through ultrasonic telemetry links. Referred to as *INtervened-Timing, Enhanced-Rate Interval Modulation* (*INTERIM*), the proposed technique is an isochronous pulse-based modulation technique, which embeds the telemetered symbol in the time interval between two consecutive ultrasonic tone bursts of different frequencies. To realize this idea, two pairs of ultrasonic transducers with different central frequencies and non-overlapping frequency responses are used. Each transducer pair oversees the transmission and receipt of one of the tone bursts. To be of short duration and at the same sufficiently time high amplitude, each tone burst is generated using the *pulse-harmonic modulation* (*PHM*) technique. The main achievement in this work (which makes it superior to the PHM technique) is making the maximum data telemetry bit rate independent from the duration of tone bursts. This allows for significant enhancement in the maximum achievable data telemetry bit rate in ultrasonic links. From among other advantages of the INTERIM approach, one can name the insensitivity to non-idealities such as noise and delay deviation.

To assess the success of the INTERIM approach, an experimental setup was developed using two pairs of transducers with 1-MHz and 5-MHz central frequencies. The transmitting and receiving transducers were placed in a tank of water with adjustable distance. According to our experimental results at a distance of 5 cm, the 1-MHz and 5-MHz PHM links could provide a maximum data rate of 70 kbps and 350 kbps, respectively. This is while using the same transducers in the same operational conditions (*i.e.*, with the same *excitatory-inhibitory pulse* (*EIP*) excitations, same link medium, and at same distance), the INTERIM approach offered a

maximum data rate of 500 kbps and 800 kbps at *bit error rate* (*BER*) of 1.4% and 6% respectively.

***Keywords:*** Ultrasonic links, data telemetry, wireless interfacing, implantable biomedical microsystems

# Dedication

To my parents.

# Acknowledgments

I would like to express my sincere gratitude to Prof. Sodagar for his unconditional support and guidance all throughout my research.

## TABLE OF CONTENTS

# List of Figures

# List of Tables

# Objective of Thesis

The main issue with ultrasonic data telemetry is the limited data rate which makes the higher data-rate applications such as image processing practically impossible. There have been major improvements from early works which were limited to tens of kilobits per seconds data rates toward hundreds of kilobits per second. The introduction of pulse-based methods has been helpful as well as the idea of using multiple transducers.

The primary goal of this project is the enhancement of the rate of data transfer through ultrasonic telemetry links with living tissues as the signal transfer medium. The limitations of ultrasonic data transfer can be better understood by most of the works done in this area over the last decade. In almost all the works, the center frequency of the transducer imposes a strict restriction on the maximum possible bit rate in data telemetry.

The main objective of this thesis is to design a platform and positioning system for multiple ultrasonic transducers, and then add some signaling techniques to come up with a modulation scheme that allows for wireless transfer of binary data at an enhanced data rate.

We aim to design and develop a new technique which uses two different frequencies to increase the data rate. We are aware of the frequency-division multiplexing technique that has been already reported in [1], but the dual-frequency technique being developed in our work is quite different in concept. Our technique uses the pulse-based modulation technique proposed in [2], and adds a second dimension in the encoding of the signal using the second pair of transducers used. Preliminary studies show that using the proposed technique can elevate the rate of the data being telemetered through the dual-frequency ultrasonic telemetry link proposed in this work.

# Chapter 1: Introduction and Literature Review

# Chapter 1: Introduction and Literature Review

## 1.1. Introduction

Recent progress in electronics and medical sciences has provided scientists and engineers with the ability to combine these two fields to help with different needs in medicine and biology. For instance, the miniaturization of electronics has made it possible for doctors to put different kinds of health monitoring, drug delivery, and stimulating devices inside the human body, and even power up such devices through wireless connection. Cardiac pacemakers and cochlear implants are among the most famous examples of the integration of electronics technology and medical sciences for the development of implantable medical devices.

The key problem with these kinds of methods is the fact that they make patients uncomfortable both because of their size and the usage of wires. Thanks to the shrinking of electronic devices and the advancement of data and power telemetry in recent years, Implantable Wireless Devices have gained more and more attentions because of their convenience and the advancement of data rate and power telemetry efficiency.

The end goal for using wireless telemetry to implants has been to form a network of implantable devices functioning together inside the body and maintaining different needs, monitoring several intrabody factors and signals and solving different bodily problems such as unfunctional organs. There is quite a long road to that destination but there has been impressive works that hint toward that future.

The main barrier towards that future seems finding a) a power source which is long-term, dependable, safe, and strong enough without the need of huge batteries and intrusive interconnects and b) an acceptable data rate towards implants for executing the external commands without being harmful to the body. There is also an additional problem with the intrusiveness of the implants but

the fact that we can now integrate millions of transistors into a millimeter-sized chip makes it possible for the scientists to do this in a safer way. But still the need for some post-reception processing may need bigger chips that could cause problems which is another area that needs further improvements.

## 1.2. Fundamentals of Ultrasonics

The primary purpose of acoustic wave is to propagate an acoustic wave by generating pressure changes and compression. This results in increased pressure changes, which promotes the propagation of acoustic waves. [3] In fact, the equations governing acoustic waves are nonlinear and complex. However, the linear approximation used in several research involving acoustic waves is a viable model and is equivalent to the electromagnetic wave equations.

Using piezoelectric materials, mechanical energy is transferred to electrical energy or vice versa. They are the most widely used and effective ultrasonic transducer available. The basic purpose of these transducers is to change their size and deform when exposed to an electrical field. Additionally, when they are subjected to physical stress, like as sonic waves, they generate electrical current.[4]

Acoustic waves propagating through a nonpiezoelectric solid medium mix longitudinal (expansion and contraction in a single path) and shear (transverse to the propagation direction) waves.

Each point on the face of the radiating transducer may be viewed independently as a point source of radiation according to the Huygens principle[5]. The pattern of the acoustic field in front of the transducer face is the vector sum of all point sources [6]. In general, the Rayleigh integral describes the pressure field at an observation point $L(x, y, z)$:

$$P(x,y,z;t) = \rho_0 \int_S \frac{\dot{u}_p\left(x',y':t-\frac{r}{c_0}\right)}{2\pi R} dS \quad (1.1)$$

where $(x', y')$ are the coordinates of a point source on the transducer; (x, y, z) are the coordinates of the observation point in front of the transducer; $\dot{u}_p$is the vibration velocity function over the radiating cross section of the transducer; $c_0$ is the average speed of sound (wave phase velocity) in the medium; $\rho_0$ is the average medium density; and S is the transducer area. R is the distance from the point source to the observation point *L*(x, y, z):

$$P(x,y,z:t) = \frac{jk\rho_0 c_0 u_0}{2\pi} e^{j\omega t} \int_S \frac{e^{-jkR}}{R} dS \quad (1.2)$$

Continuous Wave (CW) sinusoidal excitation distributed evenly across the face of a disc-shaped transmitter, where R denotes the distance between the infinitesimal point source and the observation point; $u_0$ denotes the vibration velocity amplitude; k denotes the wavelength of the pressure wave in the medium, $c_0$ denotes the phase velocity of the wave, $\rho_0$ denotes the medium density; x denotes the angular frequency, and k= $\omega$/c=2$\pi$ /$\lambda$ is the wave number. Indeed, for a dissipative medium such as tissue, the wave number k should be complex, $k^2 = \alpha^2 + \beta^2$ where $\beta$ is the phase speed $\beta = \omega/c$ and $\alpha$ is the absorption coefficient. (1.2) is solved for r>>a and CW sinusoidal excitation.:

$$P(r,\theta:t) = \frac{ja\rho_0 c_0 u_0}{r} e^{j(\omega t - kr)} \frac{J_1(ka\sin\theta)}{\sin\theta} \quad (1.3)$$

where a denotes the transducer radius, k denotes the wave number, J1 denotes the first order Bessel function, r denotes the distance between the centre of the radiating disc and the observation point, and h denotes the angle formed by the observation point and the acoustic axis ($\theta$ = 0) as it is demonstrated in Fig. 1.1.

$$D(\theta) = \frac{2J_1(ka\sin\,\theta)}{ka\sin\,\theta} \tag{1.4}$$

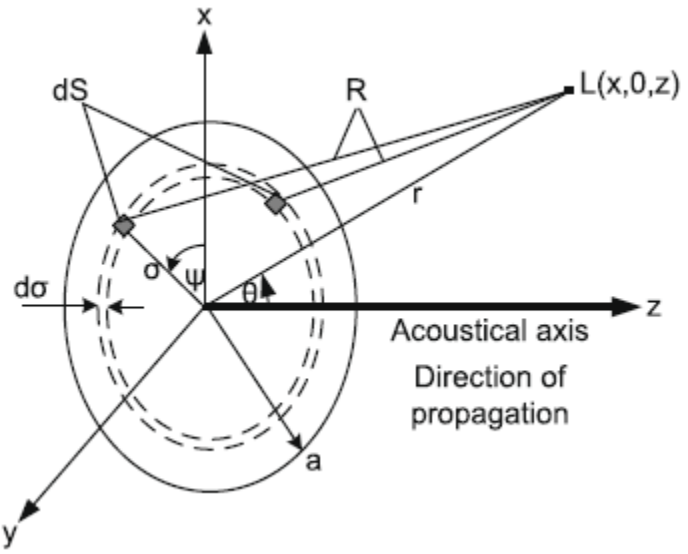


Fig. 1.1. Calculation of the pressure field generated by a disc-shaped source [5]

The transducer pressure directivity is defined as the ratio of pressure at any angle relative to the acoustic axis ($\theta$ = 0) over the same range [6] as it is shown in Fig.1.2.

The first zone, referred to as the Near Field (NF) zone, is the one that is closest to the transducer. The pressure field envelope fluctuates inside this zone, with many minima and peaks, making power transmission unpredictable as is shown in Fig.1.3.

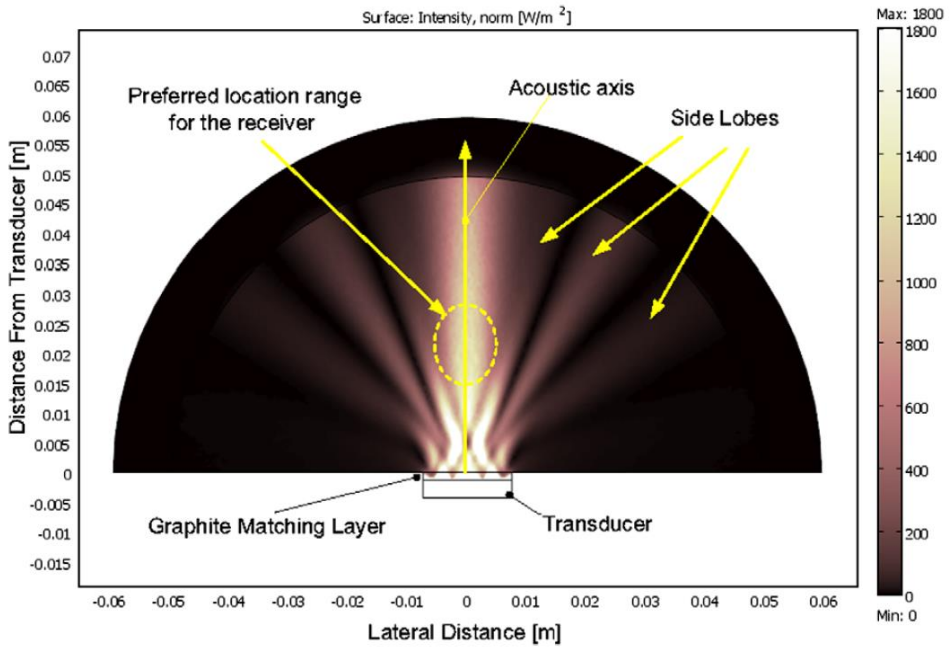


Fig. 1.2. 2D COMSOL Multiphysics simulation of a circular transducer intensity profile (radius a = 7.5 mm, $\lambda$ = 2.23 mm) [5]

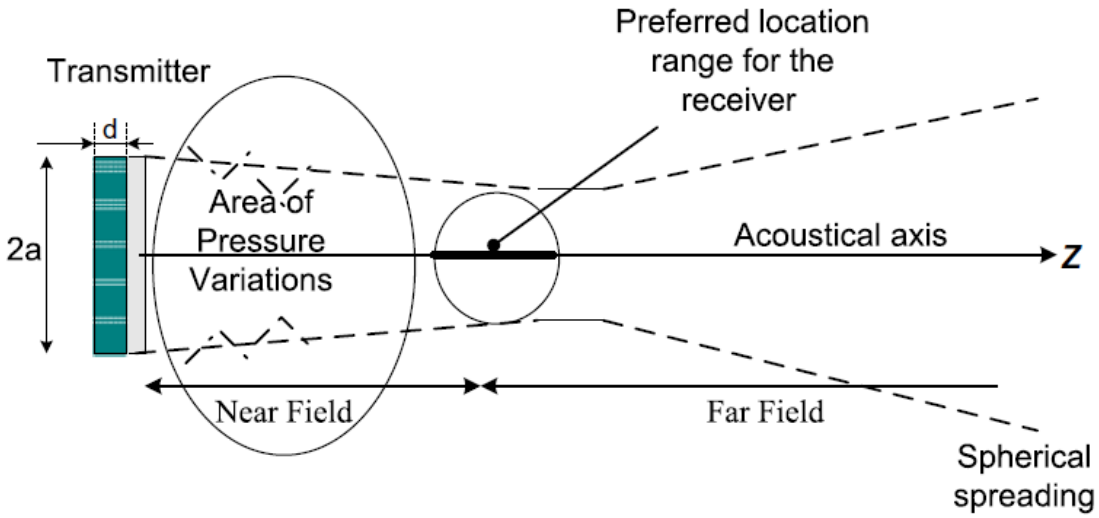


Fig. 1.3. Preferred location of implanted receiver[5]

The pressure field then aligns on a particular focus following the NF. This spacing is the ideal distance for the receiver to be located. The near field distance L from the transducer is dependent on the radius of the transducer and the acoustic wavelength k of the medium in which the wave spreads [7], and is given by:

$$L = \frac{(2a)^2 - \lambda^2}{4\lambda} \approx \frac{a^2}{\lambda} \quad \text{For } (2a^2) \gg \lambda^2 \tag{1.5}$$

Further than natural focus zone, the Far Field (FF) area begins, in which the pressure field degrades into a spherically spreading wave with minimal internal structure, whose strength decreases with distance. The acoustic axis positions at which pressure peaks rely on the wavelength and cross section of the transmitter are provided by Eq. (1.6), where m denotes the order of the pressure peak.

$$X_{\max}(m) = \frac{(2a)^2 - \lambda(2m+1)^2}{4\lambda(2m+1)} \; m = 1,2,3, \ldots \tag{1.6}$$

When the receiver must be implanted within the NF range, either a bag (1–5 mm thick) that includes acoustic jell, water, or oil can be inserted between the transmitter and the skin, or the vibration frequency can be tuned to precisely place the NF closer radiation pressure maxima on the receiver, as presented in Fig. 1.4.

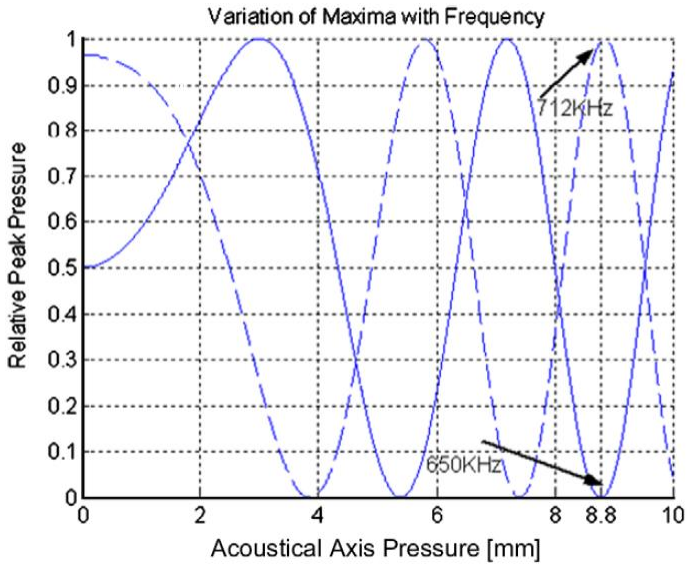


Fig. 1.4. Attaining maximum pressure at the receiver surface by frequency tuning[5]

Proper determination of the operating frequency is of great importance since it affects factors such as tissue attenuation (with a frequency dependence of f1–f1.4[8]), The thickness of the transducer, the distance to the natural focus (Rayleigh distance), and the size of the reactive components, such as inductors and capacitors, are all important considerations [9] in both the receiver and transmitter. To optimise the power output of the transducer, it is ideal to run it near to its resonance frequency. The shape and material constants of the transducer dictate the resonance frequencies. At frequencies where the thickness of the transducer equals an odd multiplication of half acoustic wavelengths, thickness vibration resonance occurs [10]. The frequency of the first resonance of a disc-shaped transducer vibrating in the thickness vibration mode (Fig. 1.5) is dictated by the thickness t and the frequency constant $N_t$ [m Hz]:

$$f_r[\text{ Hz}] = \frac{N_t}{t} \tag{1.7}$$

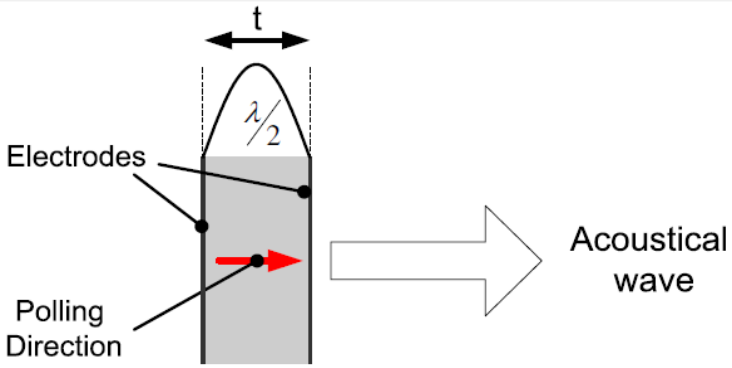


Fig. 1.5. First thickness vibration mode of piezoelectric transducer[5]

By multiplying instantaneous pressure of instantaneous particle velocity and integrating them the intensity could be calculated as:

$$I\left[\frac{W}{m^2}\right] = \frac{P_{pk}^2}{2Z} \tag{1.8}$$

where Z is the acoustic impedance of the material (tissue) that the wave propagates through. Additionally, the operating frequency impacts the quantity of acoustic energy converted to heat through tissue loss processes. Although the skin and underlying soft tissue layer have similar acoustic impedances and phase velocities to water, tissue attenuates the pressure field far more than water does (soft tissue attenuation 0.6–1.5 dB/cm compared to water attenuation 0.002 dB/cm at 1 MHz). [8], [11], and grows in proportion to the frequency and distance. Because the intensity is proportional to the square of the pressure, it lowers at double the pace at which the pressure falls:

$$I_d = I_0 e^{-2\alpha d} \tag{1.9}$$

A summary of the effect of operating frequency on design criteria is demonstrated in Fig.1.6.

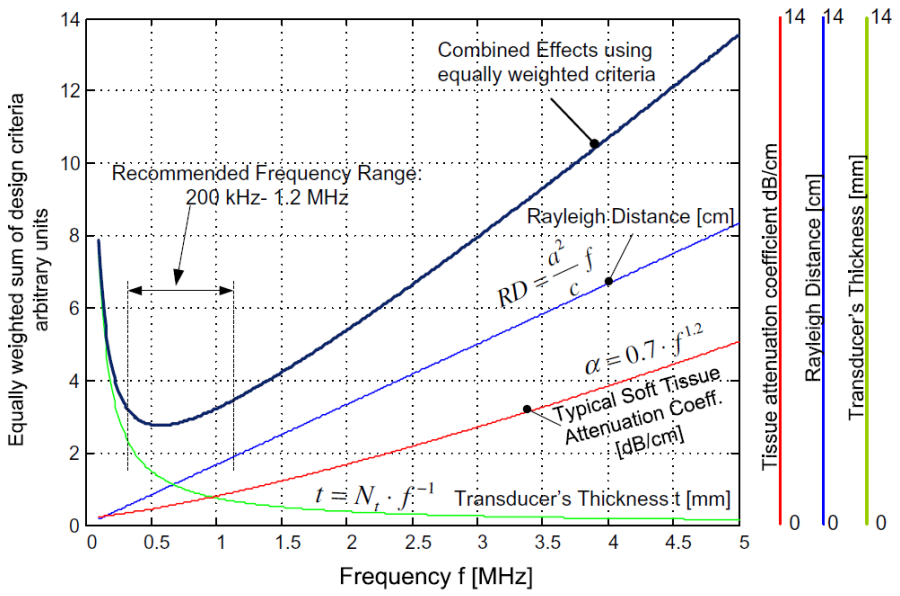


Fig. 1.6. Influence of operating frequency on design criteria, assuming transducer aperture a = 7.5 mm, c = 1500 m/s, attenuation coefficient 0.7 dB/cm at 1 MHz, and a frequency constant $N_t$ = 2020 mHz [5]

### *1.2.1. Practical Phenomena*

Path loss, noise, multi-path, Doppler spread, and a long and variable propagation delay all have a significant effect on underwater acoustic communications. [12]. All these variables contribute to the temporal and spatial variability of the auditory channel and restrict the bandwidth accessible to the Under-Water Acoustic channel (UW-A) to a small value that is highly dependent on both range and frequency. Attenuation is primarily caused by absorption because of acoustic energy being converted to heat. Attenuation is proportional to distance and frequency. Fig. 1.7 shows the acoustic attenuation for a short-range shallow water UW-A channel as a function of frequency and distance, using the propagation model described in [13].

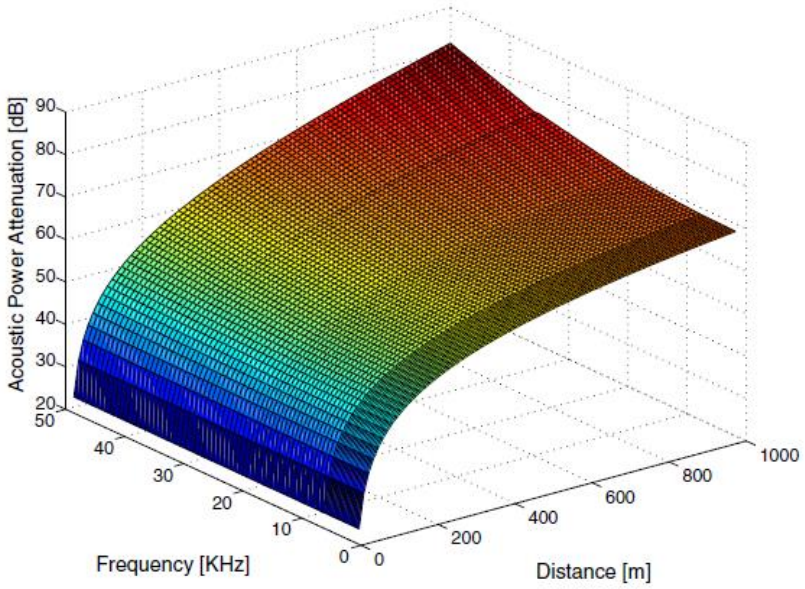


Fig. 1.7. Path loss of short-range shallow UW-A channels vs distance and frequency in [12]

Some of the main factors that influence acoustic data/power telemetry are[12]:

- Path loss: Including **attenuation** which is mainly caused by conversion of acoustic energy into heat leading to absorption and increasing with distance and frequency.\
- Noise: Which includes man made noise and ambient noise caused by blood flow and other biological phenomena.
- Delay and delay variance: delay and delay variance can cause serious error in high-rate data telemetry as it causes errors in design parameters and may cause adjacent symbols to overlap.
- Multi-path: multi-path propagation generates inter-symbol interference (ISI) and may be caused by the reflection of the original signal through different body parts.

## 1.3. Ultrasonic Transducers

The availability of appropriate transducers is one of the most important aspects in the development of ultrasonic links. Miniaturized implants are now conceivable because of the advancements in the production of millimeter or even nanometer-scale transducers.

### *1.3.1. Materials*

Due to their high electrical-mechanical coupling coefficient, which is an important factor for power transfer efficiency, and low sound velocity, that makes their typical resonance frequency in the range of a few Megahertz, which is desirable, the most common materials to be used as an ultrasonic transducer are based on Lead Zirconate Titanate (PZT) and Lead Magnesium Niobate (PMN).[1]– [5]. PVDF (polyvinylidene difluoride) is also utilized in some instances, but due to its poor electrical-mechanical coupling coefficient, it is not employed as frequently.

This equation may be used to calculate the operating frequency of an ultrasonic transducer (the range between short-circuit and open-circuit frequency): [4]

$$foc = \frac{Vp}{2t} \qquad (1.10)$$

In this case, the material sound velocity and the thickness of the transducer are critical. For example, velocity levels of approximately 5000 m/s correspond to typical values of around 1 mm thickness and 1MHz frequency. The electromechanical coupling constant relates the short circuit frequency. The impedance values for these materials at their operational frequencies are another essential characteristic to consider when choosing a material for a transducer. (These figures are

based on a typical area of 1 $mm^2$ and a thickness of 1.4 mm). These figures are significant because the resistance required for their matching circuit is close to these figures. As a result, certain materials, such as $LiNbO_3$, and PVDF are not suitable for typical implants.[19]. Some of the properties of the most common piezoelectric material is shown in Table 1.

Table 1 Properties of most common piezoelectric materials[19]

| | **PZT-4** | **PZT-5H** | **$BaTiO_3$** | **PMN-PT** | **$LiNbO_3$** | **PVDF** |
|---|---|---|---|---|---|---|
| | "Hard" Ceramic | "Soft" Ceramic | Ceramic | High-Performance Single Crystal | Single Crystal | Piezoelectric Polymer |
| Density ($kg/m^3$) | 7,500 | 7,500 | 5,700 | 7,640 | 4,640 | 1,780 |
| Sound velocity (m/s) | 4,100 | 3,850 | 5,000 | 3,560 | 6,400 | 1,109 |
| Acoustic radiation impedance, $Z_{0,p}$ (MRayls) | 30.8 | 28.9 | 28.5 | 27.2 | 29.7 | 1.97 |
| Electrical-mechanical coupling coefficient ($k_{33}$) | 0.70 | 0.75 | 0.5 | 0.91 | ~0.5 | 0.18 |

## *1.3.2. Packaging*

Packaging transducers as an alternative for utilising unpackaged ones for the usage of biomedical ultrasonic transfer has risen in recent years due to the challenges of forging a tailored transducer for each experiment. In packaged transducers, the active part of the transducer is a thin disk- usually a rectangle- of piezoelectric ceramic or composite that converts mechanical energy to electrical and vice versa. The piezoelectric material is usually protected from damage by a wear plate and backed by a block of damping material that quiets the transducer when it is generating sound pulse and this assembly is mounted in a case with appropriate electrical connections as it is shown in Fig.1.8.

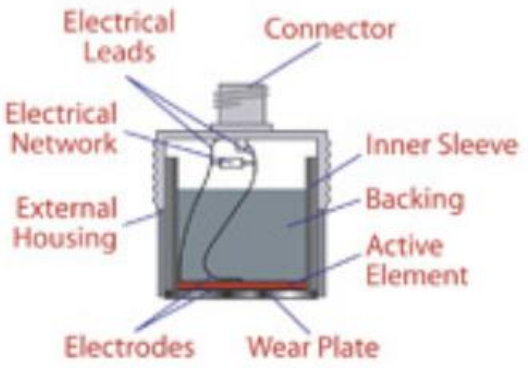


Fig.1.8. Typical packaged transducer structure[20]

### *1.3.3. Energy Conversion*

The atomic lattice structure of a piezoelectric material is asymmetric[4]. When such a material is subjected to an electric field, its mechanical dimensions are altered. In contrast, a piezoelectric material that has been stressed generates an electric field. Piezoelectricity is present in all ferroelectric materials. The crystal's positive charge centre does not correspond with its negative charge centre in the ferroelectric state, as seen in Fig. 1.9, two non-identical nearby atoms will not travel the same lengths in response to an applied electric field in such a material. As a result, when an electric field is given to a ferroelectric material, the substance's dimensions change (i.e., the material is stretched).

As an example, consider the periodic atomic system shown in Fig.1.9, where $a_1$ and $a_2$ are the equilibrium spacings between adjacent rows of atoms in the z direction, and the equilibrium spacings in the x and y axes between adjacent rows of atoms are l.

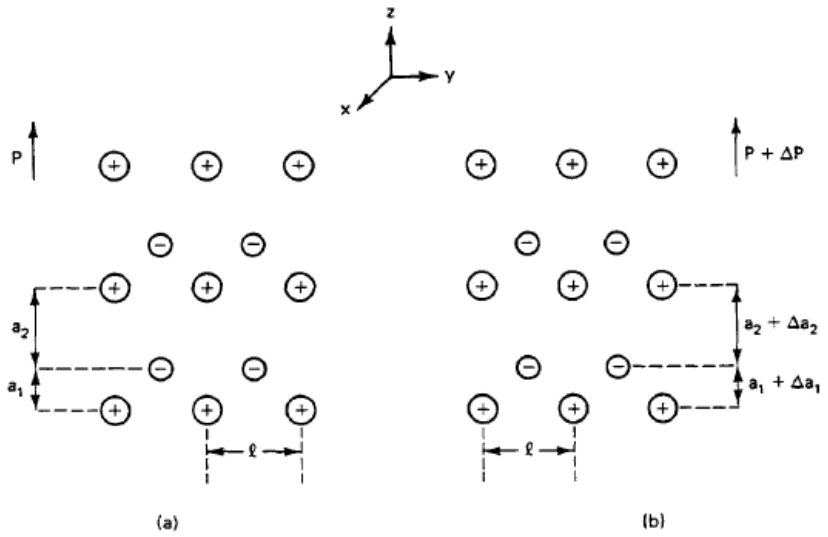


Fig.1.9. Ferroelectric crystals: (a) unstrained; (b) strained [4]

The dipole moment per unit volume of these atoms is:

$$P = \frac{q(a_2 - a_1)}{l^2(a_2 + a_1)} = \frac{\text{dipole strength of unit cell}}{\text{volume of unit cell}} \tag{1.11}$$

where q and -q are the charges on the atoms, respectively. We will now investigate the influence of strain on the material's polarization. When $a_1$ becomes $a_1 + \Delta a_1$ and $a_2$ becomes $a_2 + \Delta a_2$, the polarization of the system changes by $\Delta P$, and we may also write $\Delta a_1 = a_1 S$ and $\Delta a_2 = a_2 S$. As a result of Eq. (1.2), the first order in strain becomes:

$$\Delta P = PS = eS \tag{1.12}$$

where e denotes the piezoelectric stress constant and S denotes the macroscopic strain present in the material.

In the presence of an electric field, the overall change in electric displacement is as follows:

$$D = \varepsilon E + \Delta P \tag{1.13}$$

We can also write:

$$D = \varepsilon^S E + eS \tag{1.14}$$

where the dielectric constant denotes the permittivity at zero or constant strain and is represented as $\varepsilon^S$. In a piezoelectric material, the electric displacement is proportional to both strain and electric field.

We will now calculate the stress caused by an electric field E in a piezoelectric material. Positive and negative atoms have forces per unit area of $qE/l^2$ and $-qE/l^2$, respectively. Thus, the stresses in the length $a_2$ and $a_1$ regions are as follows:

$$T_2 = \frac{qE}{l^2} \tag{1.15}$$

and:

$$T_1 = -\frac{qE}{l^2} \tag{1.16}$$

respectively. As a result, the average stress in the medium because of the electric field is as follows:

$$T_E = \frac{a_1 T_1 + a_2 T_2}{a_1 + a_2} = eE \tag{1.17}$$

The total stress applied to the medium is equal to the sum of the externally applied stress T and the internal electric field-induced stress $T_E$. Hooke's law results in the following:

$$T + T_E = c^E S \tag{1.18}$$

or

$$T = c^E S - eE \tag{1.19}$$

where the elastic constant is defined as $c^E$ in the presence of a constant or zero E field. Equations (1.5) and (1.10) are referred to as the piezoelectric constitutive relations. We may estimate the value of $e$ by assuming that $a_1 = 2$Å, $a_2 = 4$Å, and $l = 3$Å, and taking $q$ to

be the charge of a single electron; these assumptions results in an estemiate of $e = 0.6\mathrm{C/m^2}$. Due to the fact that atoms can have multiple charges, this value is significantly less than the highest measured values of e in strongly piezoelectric materials such as lead zirconium titanate (PZT) ceramics($e_{z3} = 23.3\mathrm{C/m^2}$ in PZT-5H) or lithium niobate crystals, but it is similar to values recorded in a wide variety of other piezoelectric materials.

### *1.3.4. Electrical Considerations*

In Sec. 1.2. we observed that there are relatively rapid variations in the "preferred location ranges from the receiver" and slower variations in the "far-field". These field fluctuations are created by the phase discrepancies between the rays of acoustic waves arriving at a given spot from various points on the surface of a transducer. [4] analyses and establishes that when a transducer is activated with a brief pulse (one or two central frequency cycles in duration), certain cancellations and additions vanish, and the response becomes smoother. For example, the nulls that appear in the case of a continuous wave signal are replaced with minima in the pressure profile and the variation becomes smoother.

### *1.3.5. Transducer Modeling*

For us to understand the relationships between the mechanical and the electrical territories of the piezoelectric materials, a simple yet realistic model is needed that involves mechanical strain and stress and electrical field. The most used model is called the KLM model by Krimholtz, Leedom, and Matthaei [21] but there are other models such as Mason Equivalent Circuit[22], [23] and Redwood Equivalent Circuit [24] that have some merit. This model works for devices in the shapes like thin plates and considers them as one-dimensional. This model considers the material as a

three-port network that has two acoustic ports and on electrical port. It also relates the force F to voltage and the velocity v to current and includes acoustic impedances that help with employing matching networks to increase efficiency of the ultrasonic transfer. The equivalent circuit is shown in Fig.1.10.

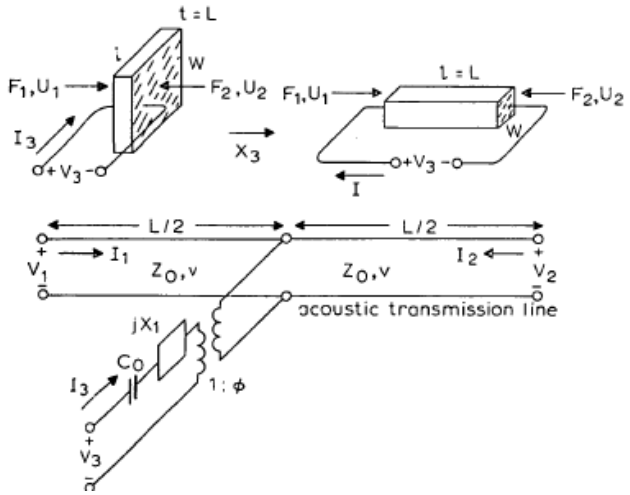


Fig.1.10. Equivalent circuit for thickness-expander plate [21]

There are techniques that utilize this model to increase efficiency of the link. Using air as a backing material helps in removing the back port of this model which is demonstrated in Fig.1.11. Because of the low acoustic impedance of air which is orders of magnitude smaller than the acoustic impedance of transducers, using air helps convert all the mechanical energy into electrical energy and as a result increasing the efficiency.

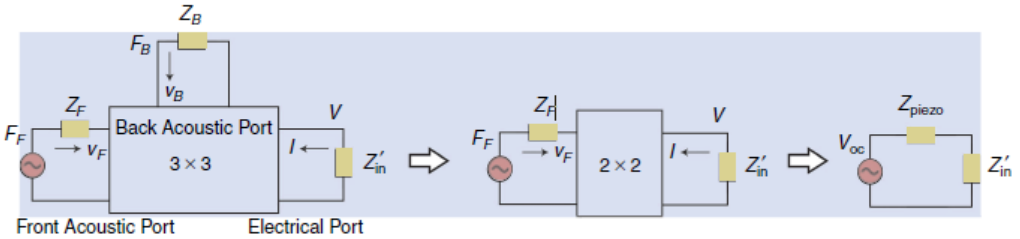


Fig.1.11. Effect of using air as a backing material [19]

## 1.4. Computer-Aided Design and Simulation Tools

A very useful simulation tool for acoustic waves is COMSOL. A demonstration of this tool's use is presented in Fig.1.12, which depicts a two-dimensional finite element simulation of the pressure intensity profile created by a disc transducer.

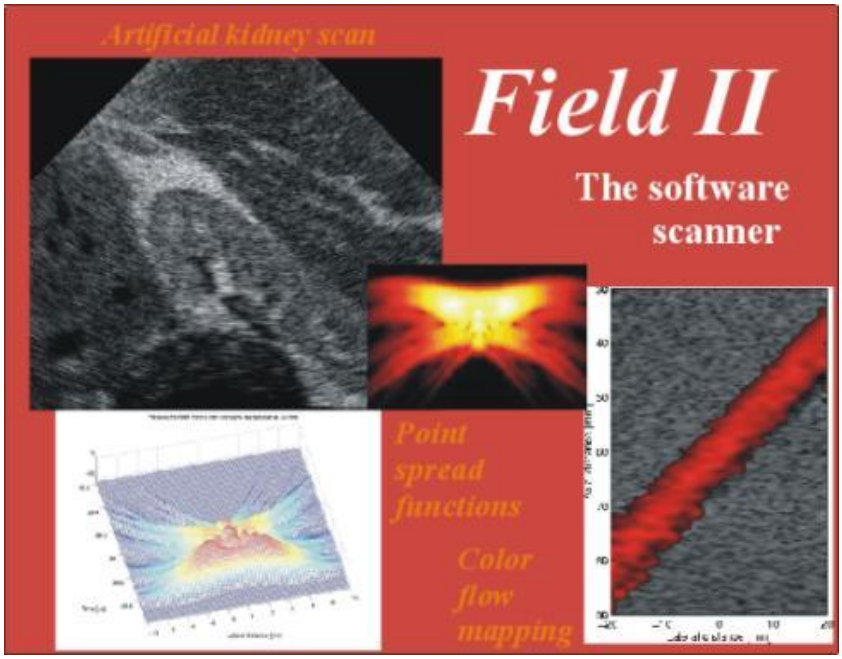


Fig.1.12. FIELD II simulation tool

Another useful tool for modelling ultrasonic transducer fields and imaging using linear acoustics is FIELD II [25], which calculates pulsed ultrasound fields using the Tupholme-Stepanishen approach.

## 1.5. Standards

For an implant to be permitted by the U.S. Food and Drug Administration (FDA), a limit must be considered. An excessive intensity could harm body tissue and cause damage. To prevent that the permitted spatial peak temporal average intensity (ISPTA) of diagnostic ultrasound systems must be held under 720 mW/cm$^2$ [25]. This gives ultrasonic diagnostic systems an advantage over other

methods like RF which has a limit of up to 1mW/cm$^2$, and as a result makes it much more superior in terms of power transfer to implant.

There are other standards that serve more as recommendations for specific purposes such as IEEE Guide for Medical Ultrasound Field Parameter Measurements [26] and IEEE Standard Terms and Definitions for Surface Acoustic Wave (SAW) Devices [27].

# Chapter 2: Review of Telemetry Links for Implantable Biomedical Microsystems

# Chapter 2: Review of Telemetry Links to Implantable Biomedical Microsystems

## 2.1. Introduction

Typically, an IBM is connected to an external host through a wireless connection. To keep the complexity and size of an implant to a minimum, most signal processing units are retained external to the body and placed in an external host. Additionally, the external host transmits the power required for the implant modules through wireless interfacing. Moreover, the wireless connection is utilized to transport data bidirectionally between the implanted device and the outside world. Thus, the implant wireless interface must include a power regulator, a demodulator for receiving control/programming data (forward data telemetry), and a modulator for transmitting recorded signals and implant status to an external host (reverse data telemetry). A general concept of the telemetry link is demonstrated in Fig.2.1.

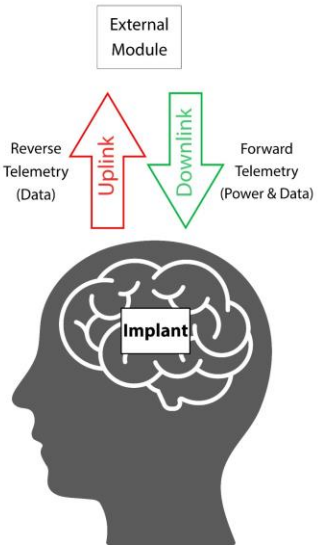


Fig. 2.1. A general look at the telemetry link

## 2.2. Telemetry Links

Before diving deeper into the ultrasonic links, more traditional methods should be discussed. These methods are mostly based on electromagnetic energy, and they include capacitive, inductive, and radio frequency (RF) methods.

### *2.2.1. Inductive Links*

They are mostly implemented by two closely spaced, inductively linked coils that serve as the primary wireless connection for forward power and data telemetry. The secondary coil is implanted inside the body, while the first coil is preserved outside. Typically, these coils are a few millimeters apart, separated by thin layers of live tissue. Normally, both ends of the connection are tuned to the same resonance frequency in this configuration to maximize power transmission efficiency. The carrier frequency is restricted to a few tens of megahertz to allow for the passage of substantial quantities of energy to the implant.

This is because power dissipation in tissue, which results in an excessive temperature rise, grows exponentially with carrier frequency squared. In summary, although these links have a high-power efficiency, they are weak in long distances, suffer from high attenuation and crosstalk effect.

### *2.2.2. Capacitive Links*

Capacitive links are made up of two parallel plates that are capacitively coupled. One plate is linked to the implant and the other to the skin on the exterior side. The plates are positioned to maximize their overlap, while the skin and thin layers of tissue serve as a dielectric. In this strategy, the electric field serves as the carrier of energy and data, in contrast to the usual inductive approach, which relies heavily on the magnetic field. Capacitive links have many advantages over inductive

links such as higher data rate, high-pass frequency response and multi-path transmission but they are weak in long distances which causes problems with deeper implants.

### *2.2.3. Ultrasonic Links*

Ultrasonic Links are implemented using two or more ultrasonic transducers transmitting and receiving data and power. Because of the less harmful nature of ultrasonic waves to human tissue, ultrasonic telemetry has the potential for a higher power transmission. In the next section, the two main domains of ultrasonic telemetry (power and data) are going to be investigated.

## 2.3. Ultrasonic Power Transfer

Some of the major works in the ultrasonic telemetry field has been done in the power telemetry side; Although it is not the major focus of our research, it can give us a better understanding of the reason for the recent growth in focus on the field. As a result, different aspects of this field such as its applications, the link medium, and its affect on the telemetry, the circuitry and the recent advances are going to be studied in this section.

### *2.3.1. Applications*

Because ultrasonic wireless power transmission can pass into deep tissues, it has been employed in a growing number of applications in recent years. Other advantages include a high misalignment tolerance, a wide penetration range, and higher efficiency than inductive methods. Furthermore, the ultrasonically powered implants are excellent for in depth brain stimulation due to their practicality in being used in micro-scale devices. Visual prosthesis [15], neuromodulation

[28], optogenetics [17], neural stimulation [29], drug delivery [30], and a variety of other applications are just a few examples which is presented in Fig.2.2.

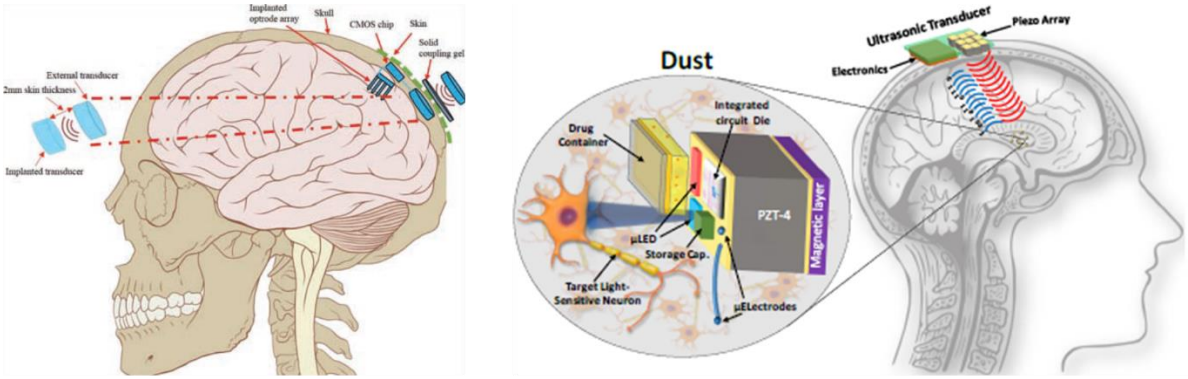


Fig.2.2. Ultrasonic power transmission applications in (a) Visual Prosthesis [2], (b) Optogenetics for Parkinson's Diseases [4]

### *2.3.2. Link Medium*

The medium in which these tests are carried out is significant since the ability of this medium to imitate the acoustic features of the human body is crucial in the experiment. In these experiments, a variety of media are used. Ex vivo experiments using pork [31] and other tissues, as well as in vivo experiments on tumours [31] and animals, are carried out in vitro using water [32], saline [1], mineral oil [33], as well as ex vivo experiments using pork [20] and other tissues and in vivo experiments on tumours [31] which is shown in Fig.2.3.

Water is an excellent choice since it makes up a large percentage of the body and may imitate its acoustic characteristics. Some of these critical characteristics are included in Table 2.

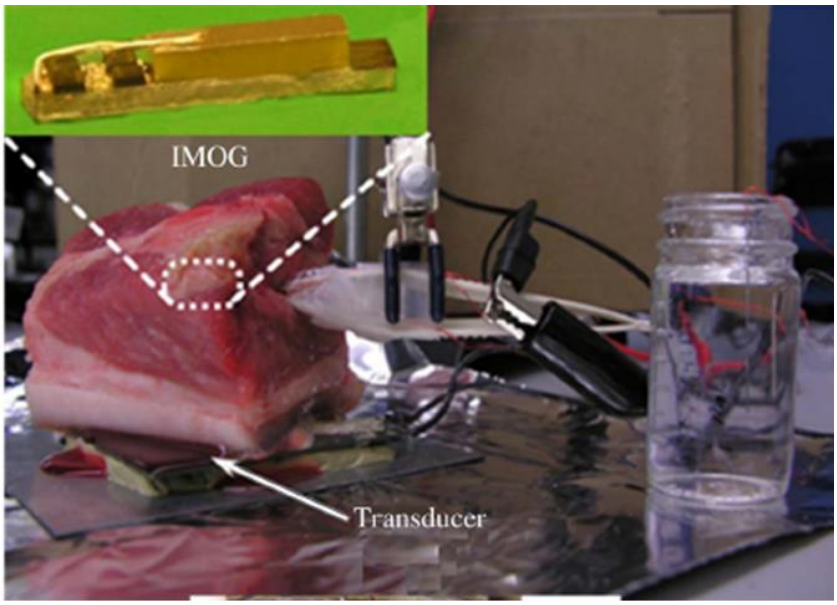


(a)

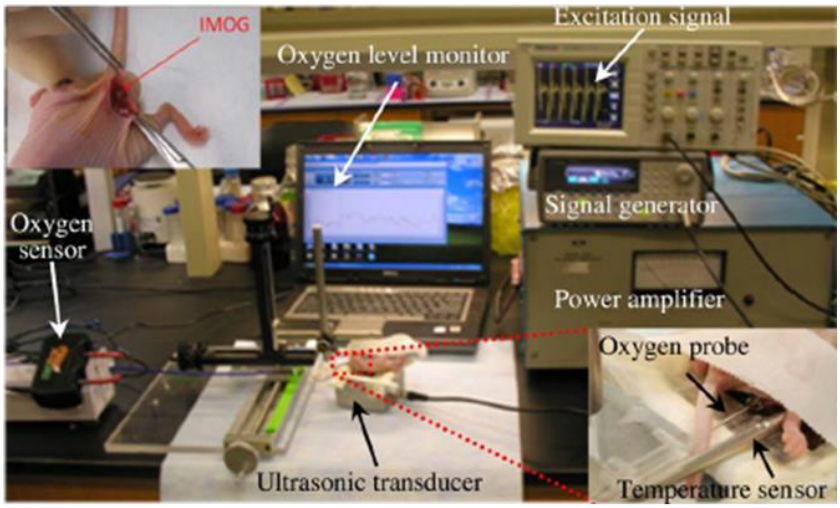


(b)

Fig.2.3. (a) Ex vivo experiments using pork [10], and (b) Real-time in vivo oxygen measurements during tumor oxygenation [31]

As it can be observed, most of the tissues have analogous speed of sound and acoustic radiation impedance(which comes into factor in matching circuitry which will be discussed later) because they are mostly made of water. The other important factor, α is the attenuation coefficient and depends on the frequency as it is shown. The attenuation can be calculated by:

$$I = I_0 e^{-\alpha z} \quad (2.1)$$

Table 2 Acoustic properties of water and important tissues and bones[19]

| Material | Density (kg/m³) | Velocity (m/s) | Acoustic Radiation Impedance (MRayls) | Attenuation Coefficient $\alpha = af^b$ | |
|---|---|---|---|---|---|
| | | | | $a$ (dB·cm$^{-1}$·MHz$^{-b}$) | $b$ |
| Water | 994 | 1,500 | 1.49 | 0.0022 | 1.0 |
| Blood vessel wall | 1,101 | 1,570 | 1.73 | 0.61 | 1.0 |
| Bone (cancellous) | 1,178 | 2,117 | 2.50 | 4.08 | 1.2 |
| Bone (cortical) | 1,908 | 3,514 | 6.71 | 4.74 | 1.0 |
| Brain | 1,045 | 1,546 | 1.62 | 0.59 | 1.3 |
| Cerebellum | 1,045 | 1,537 | 1.61 | 0.34 | 1.6 |
| Fat | 911 | 1,440 | 1.31 | 0.38 | 1.1 |
| Kidney | 1,066 | 1,554 | 1.66 | 0.24 | 1.0 |
| Large intestine | 1,088 | 1,500 | 1.63 | 0.50 | 1.0 |
| Muscle | 1,090 | 1,588 | 1.73 | 0.62 | 1.1 |
| Nerve | 1,075 | 1,730 | 1.75 | 1.15 | 1.1 |
| Tendon | 1,142 | 1,750 | 2.00 | 1.26 | 1.2 |

### *2.3.3. Driving and Supporting Circuitry for Power Transfer*

To transmit signals properly to receivers. There typically exists oscillators and amplifiers. Some driving circuitries simply contain these two parts like in [15]. In some cases, special innovations may be used to optimize the power transfer efficiency like in Fig.2.4. in which an additional inductive link is used to increase the efficiency [34]

In some cases, the driving circuitry contains a matching layer to match the ohmic impedance of the power amplifier to the imaginary impedance of the transducer. As is demonstrated in Fig.2.5, since there are less constraints in the matter of size for the driving circuitry a simple matching circuitry is employed [31].

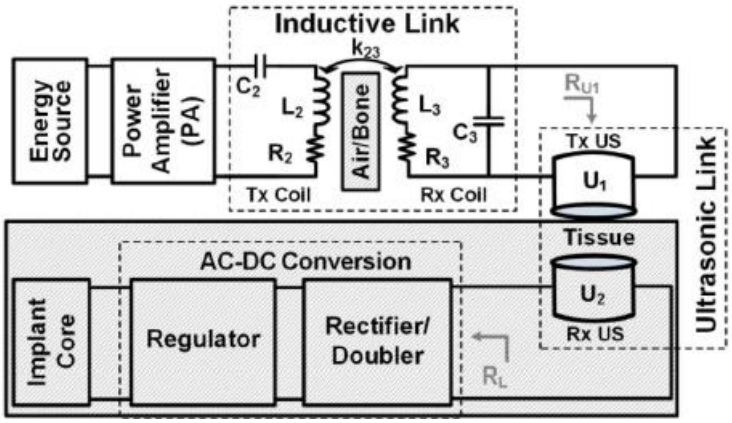


Fig.2.4. Hybrid link [34]

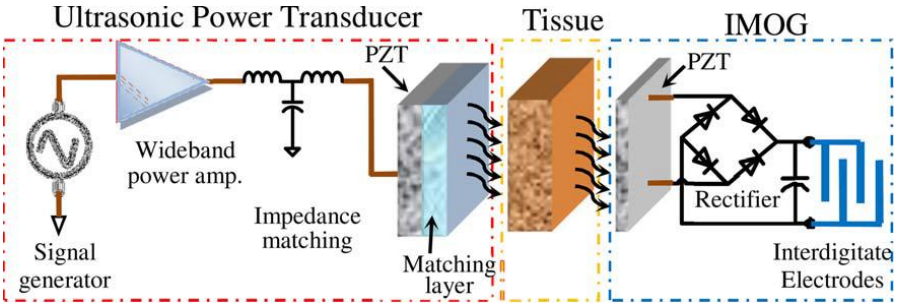


Fig.2.5. Employing matching layer in driving circuitry [31]

A very important task of the driving circuitry is the modulation. To transmit the data in a specific frequency, it must be modulated first and the sent to the implant. The circuitry differs depending on the modulation scheme but because of the size freedom we have on the external side, it can be much simpler than the circuitry employed on the implant.

Supporting circuitry which mostly consists of data recovery[35], power recovery and in some cases processors[36]. The data recovery part mainly contains demodulators, and the power recovery part includes AC/DC convertors, matching networks, rectifiers[37] capacitors for storage and even special purpose blocks like overvoltage protection [38]. Depending on the application the processing differs but the main groups contain modulators for uplink data transfer.[39]. A typical implant and supporting circuitry are presented in Fig.2.6.

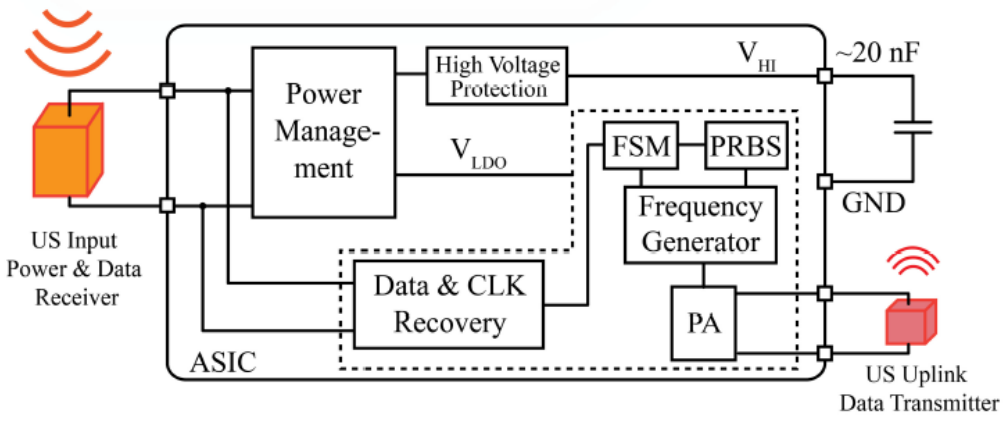


Fig.2.6. A block view of a typical implant and supporting circuitry [40]

More extensive explanation into different parts of the circuitry we first have our power recovery. The main part of most of our power recovery circuits are rectifiers and AC-to-DC converters. Some of the works use the conventional diode-based rectifier [41] but active rectifiers are also used to increase the power conversion efficiency. In [36] an active rectifier including a half wave rectifier, a comparator and a switch is demonstrated with a power conversion efficiency of 82.45% whereas a more modern rectifier is used in [37] with a power conversion efficiency of 94.51% by decreasing the propagation delay of the comparators and by reusing the consumed power by the active diodes. Another part that is demonstrated in some of the works are regulators. They are used mainly for the implants that need different voltage levels for different blocks. In Figure 6 the regulator used in [35] is demonstrated which in this work is used to generate voltage levels of 2.5V and 3.3V and in [37] a double-pass regulator is used for a stable low-noise output voltage of 1.4V.

Modern CMOS transistors, which use less power and are tiny in size, provide another problem. Because these transistors are more sensitive to higher voltages, specific overvoltage safety circuitry is required. [42] proposes a basic circuit, and [38] describes a more complicated architecture that regulates the output voltage by using the relationship between the extracted voltage and the load current which is shown in Fig.2.7.

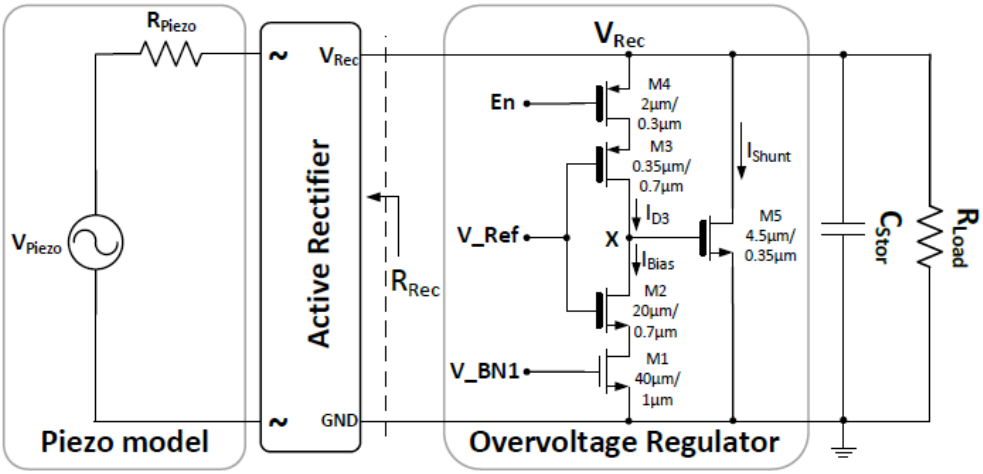


Fig.2.7. Overvoltage regulator in [38]

## *2.3.4. Recent Advances*

In recent years, many works have been put forward to improve ultrasonic wireless power transmission. In [43], the optimal geometries of the ultrasonic transducers-including their diameter and thickness for a given load and powering distance is studied. Additionally, the optimal operation frequency is studied. All these parameters are calculated through recursive design procedures to maximize power transmission efficiency.

In [44] multi-ring ultrasonic transducer is introduced; This novel transducer can focus the transmitted ultrasonic wave at different depths without the need for any lens or air cavity which is shown in Fig.2.8. Moreover, this method is helpful to enable powering multiple implants at different depths.

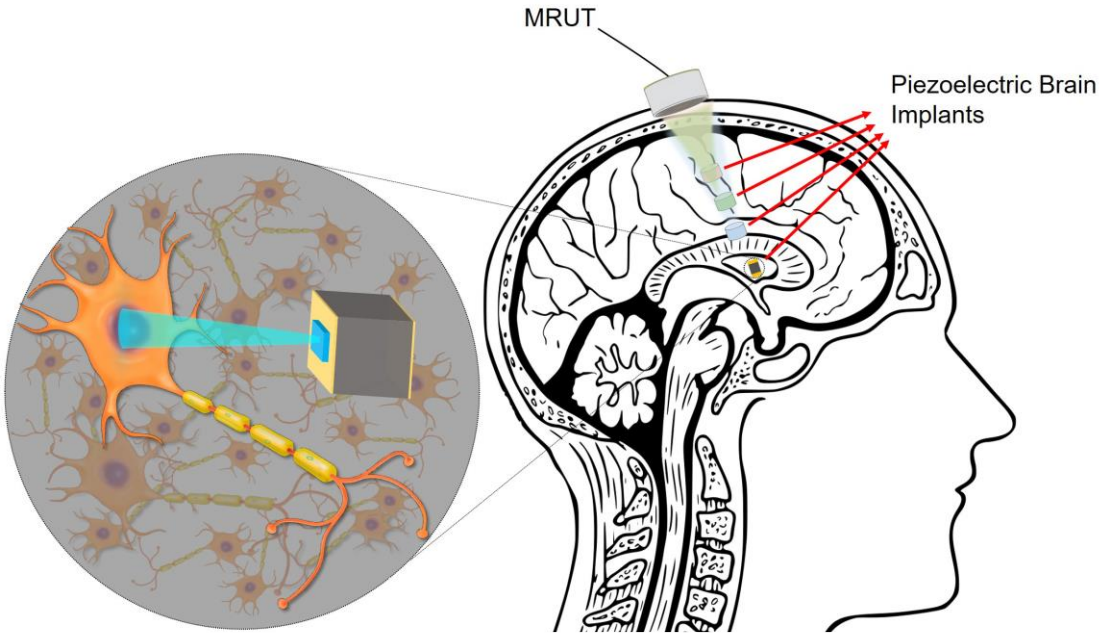


Fig.2.8. Multi-ring ultrasonic transducer in [44]

In [45], two methods are introduced for efficiently localizing ultrasonic implants. The importance of these methods lies behind the fact that small changes to implant location can have a huge impact on the ultrasonic power which is transferred. To do that, two methods called active uplink and passive harmonic backscatter are introduced and the result are compared as is demonstrated in Fig.2.9.

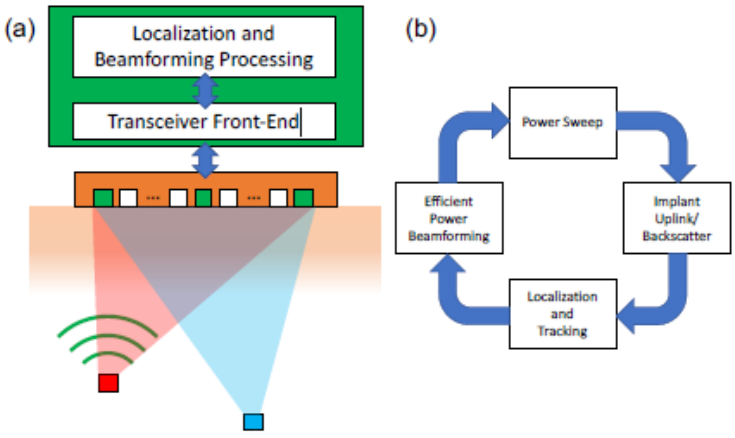


Fig.2.9. Localization system in [45]

## 2.4. Ultrasonic Data Transfer

As the focus of this work, this section is going to investigate different aspects of ultrasonic data transfer; At first, most used methods for ultrasonic data telemetry and their applications in different works are introduced. Then, the supporting circuitry for some of the works are reviewed and at the end, the most performance measured which help us better analyze and assess works in the field are studied.

### *2.4.1. Data Transfer Methods*

In this section, the two categories of digital data telemetry which are carrier-based, and pulse-based data telemetry are investigated. These methods are widely used across other fields like telecommunication as well and are well known techniques.

#### *2.4.1.1. Carrier-based Data Transfer*

There are three main carrier-based techniques for ultrasonic data transfer, and they are shown in Fig.2.10 [46]:

**Amplitude shift keying (ASK):** The carrier phase and frequency remain constant, but the amplitude alternates between two values indicating 0 and 1.

**Phase Shift Keying:** In phase shift keying (PSK), the carrier amplitude and frequency stay constant, and the phase shifts between 0 and 180, representing 0 and 1, are used.

**Frequency shift keying (FSK):** The carrier amplitude and phase remain constant, but the frequency alternates between two values indicating 0 and 1.

***On-off Keying (OOK):** A special case of ASK (or FSK) in which the values representing 0 are 0 and thus save power.

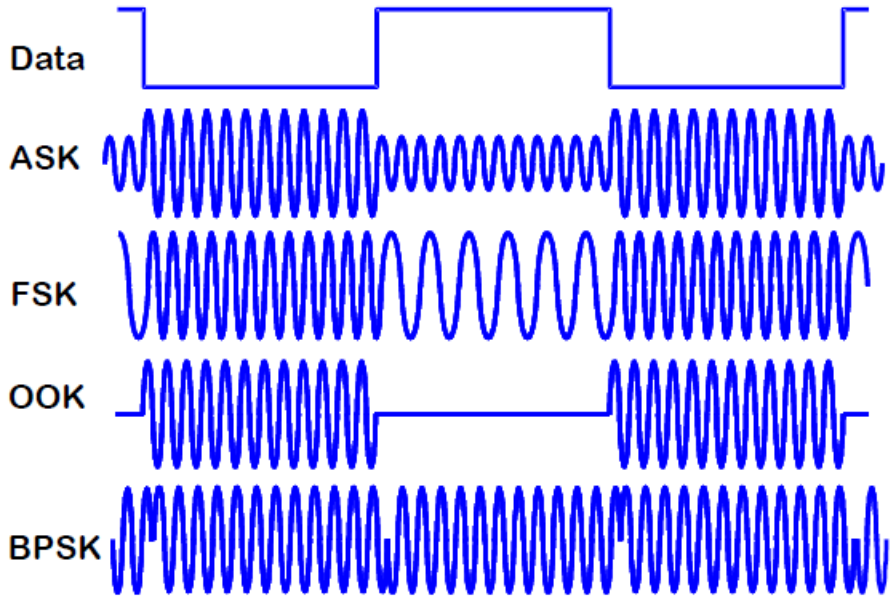


Fig.2.10. Carrier-based data transfer methods [47]

Most of the works conducting data transfer use carrier-based methods. The primary works using these techniques had low bit rates (~10kbps) [27], [44] but recent works have higher bit rates (~100kbps) [14]. These methods could be combined with other techniques to produce higher bit rates [35] or in an array to enhance their bit rate [33].

#### *2.4.1.2. Pulse-based Data Transfer*

Pulse modulation is a well-known data transmission method that employs pulses to transmit data over a channel[46].

- ***Pulse-Amplitude Modulation (PAM):*** In PAM the pulses have different amplitudes in proportion to their respective sample values as it is shown in Fig.2.11.
- ***Pulse-Width Modulation (PWM):*** Pulse-width modulation is a scheme in which the duration of individual pulses is varied based on the samples of the message signal.

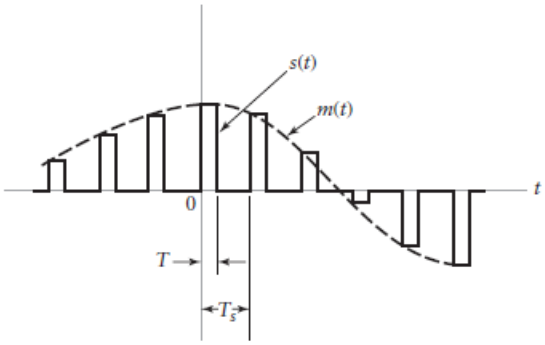


Fig.2.11. Pulse-amplitude modulation [46]

- ***Pulse-Position Modulation (PPM):*** Pulse-position modulation is an alternative to PWM where instead of using the width to send the message which make pulses long and uses considerable power, only time transitions are preserved. It can be observed this in Fig.2.12.

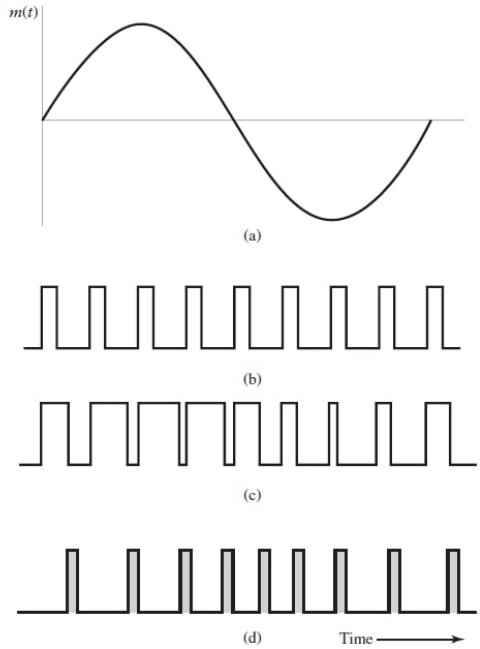


Fig.2.12. Two different pulse modulation schemes (a) Modulating wave (b) Pulse carrier (c) PWM (D) PPM [46]

- ***Pulse-Code Modulation (PCM):*** In PCM, the signal is represented discretely in both time and amplitude by a sequence of coded pulses. PCM includes a lot of techniques including Delta Modulation (DM) in which the signal is compared to its approximation and rises or

falls by Δ based on whether it is higher or lower than the approximation as is showed in Fig.2.13.

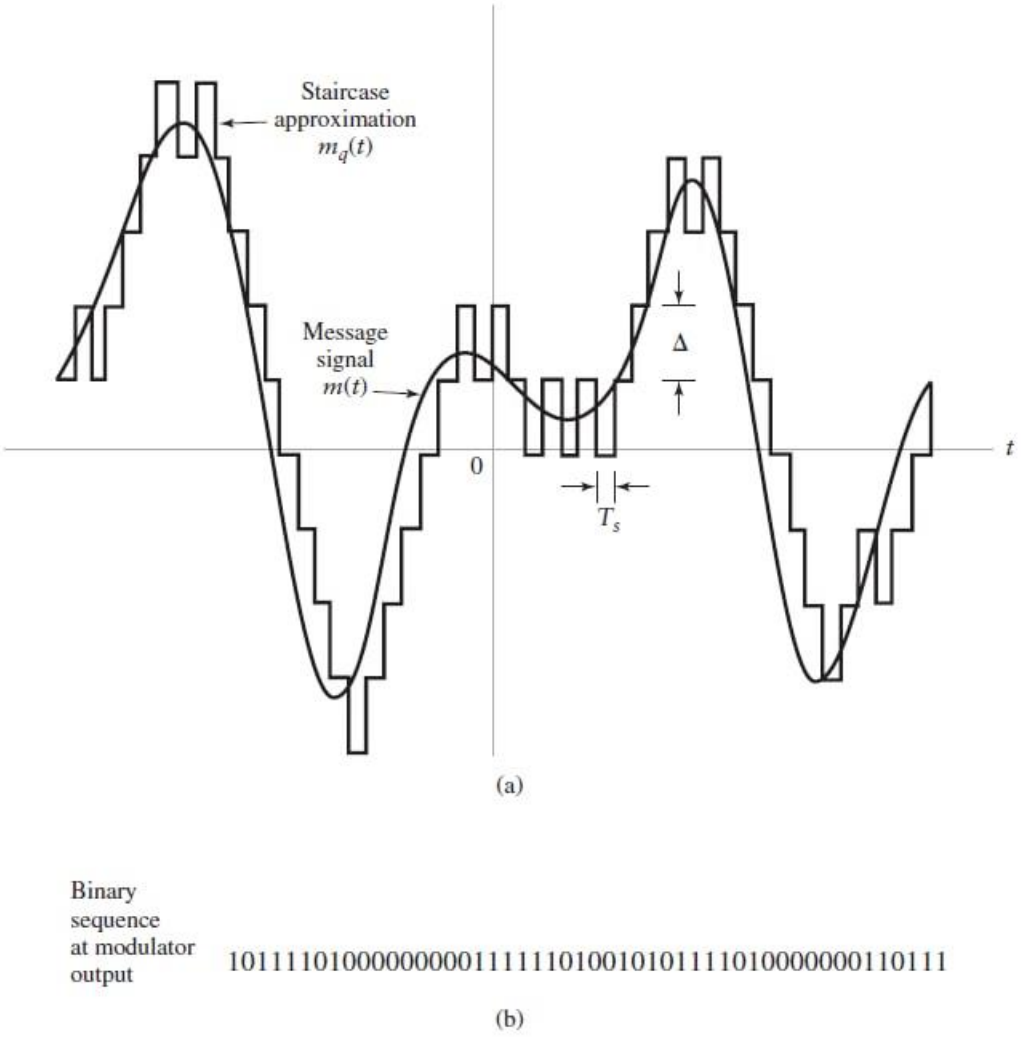


Fig.2.13. Delta modulation. (a) Input waveform m(t) and its staircase approximation and (b) the generated output sequence [46]

Because of its superior error performance, pulse code modulation (PCM) is favoured over other pulse modulation techniques (such as pulse-width modulation, pulse-amplitude modulation, and pulse-position modulation) [46]. The bandpass frequency characteristics of ultrasonic transducers are a limiting issue in realising the PCM method for high-rate data telemetry over an ultrasonic link.

An ultrasonic transducer provides an oscillating response with a natural frequency equal to the transducer resonance frequency when stimulated by a single rectangular pulse. Following the conclusion of the excitation pulse, this reaction progressively fades (referred to as the residual tail, hereafter). The major limiting issue in recommending pulse-based ultrasonic data telemetry as a suitable choice for high-rate data exchange with biomedical devices is the residual tail [2].

There has been works both using pulse positioning modulation (PPM) [49] and pulse harmonic modulation (PHM) [2] which in the latter notable bit rate of 350kbps is demonstrated in Fig.2.14 and BER performance of the link has been improved.

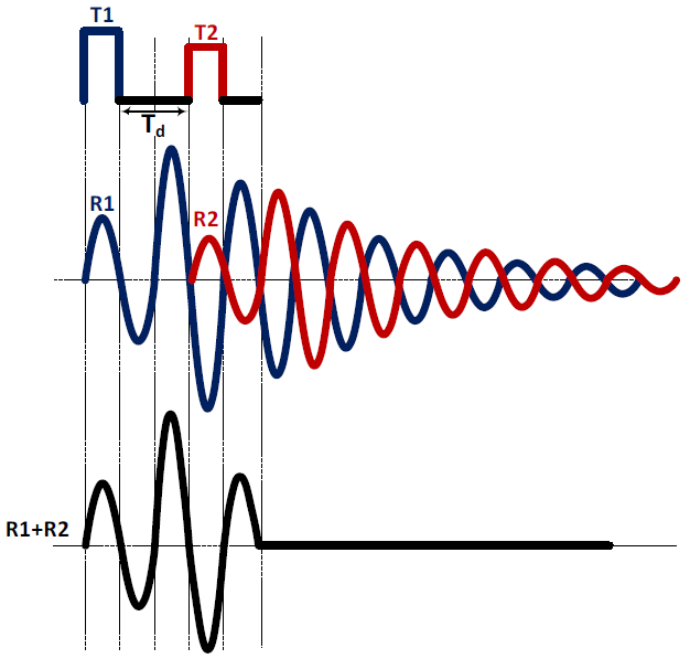


Fig.2.14. Use of an inhibitory pulse to remove the tail of resonation according to the superposition effect [2]

***Data Transfer based on Multiplexing Methods:*** Frequency division multiplexing, temporal division multiplexing, and spatial division multiplexing are examples of these techniques. The most frequently utilized is frequency division multiplexing (FDM), which has received a lot of

attention in recent research. Some notable works have been conducted in this field in which bit rates as high as 340 kbps were reached [1], [50] as it is shown in Fig.2.15.

In [14], the three kind of division multiplexing methods were experimented in a link and compared to each other.

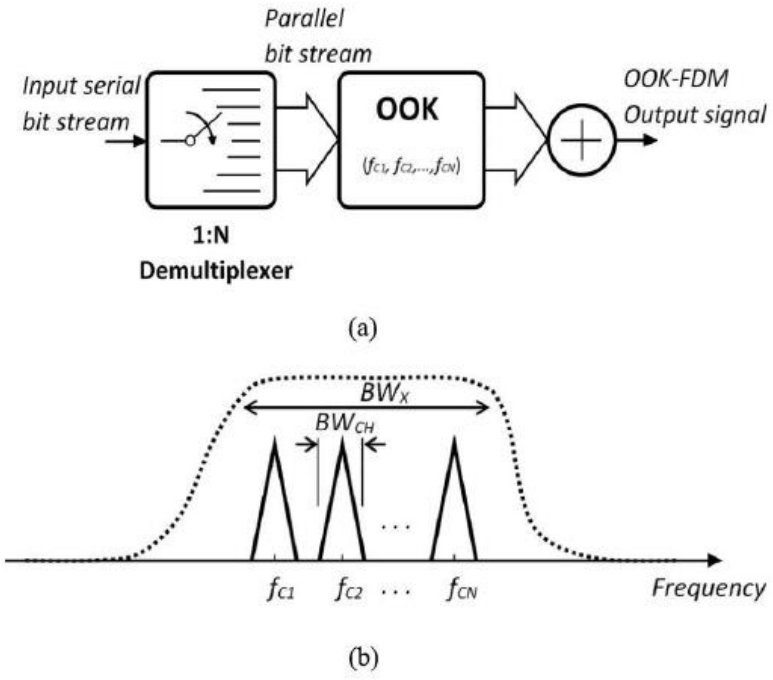


Fig.2.15. The proposed OOK-FDM idea (a) Block representation (b) Illustration of the accommodation of multiple bit streams inside the passband of the link[1]

***Hybrid Data Transfer:*** In certain works, the uplink and downlink contain distinct types of connections. The data rate required for the uplink in some applications is on the order of Mbps, which cannot be achieved utilizing solely ultrasonic lines. [42] employs an ultrasonic downlink and an RF uplink as demonstrated in Fig.2.16.

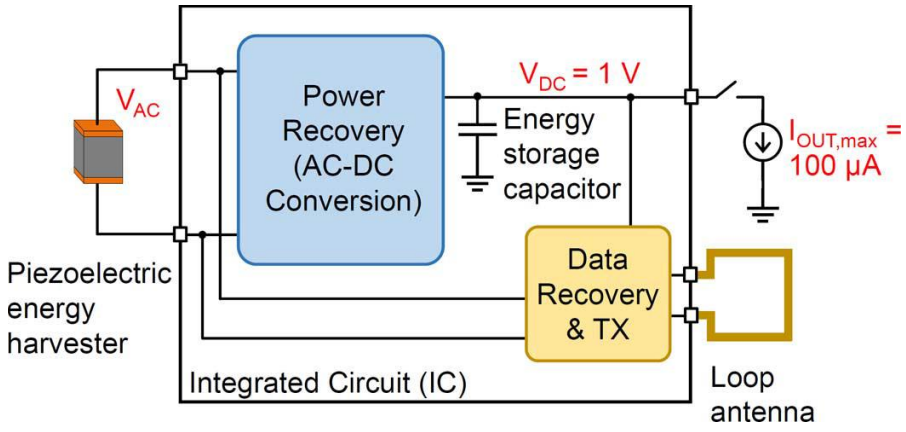


Fig.2.16. System block diagram of a hybrid implant [42]

### *2.4.2. Data Transfer Supporting Circuitry*

After the data is sent from the transmitter to the implant, it must be retrieved in a form that the implant can utilize to complete the task. As a result, depending on the modulation technique, certain circuitry is required to assist with data recovery. Most of these recovery activities also incorporate clock recovery. Fig.2.17 shows an early study based on OOK-PM signalling with the potential to restore data and clock [35]. An envelope detector, a clock recovery circuit, and a data recovery circuit are all part of this project.

A different form of envelope detection is demonstrated in Fig.2.18 which reuses the comparator in the active rectifier and as a result combines two blocks saving area and power [42]. This work uses the falling edge of the ultrasonic input as data for this link.

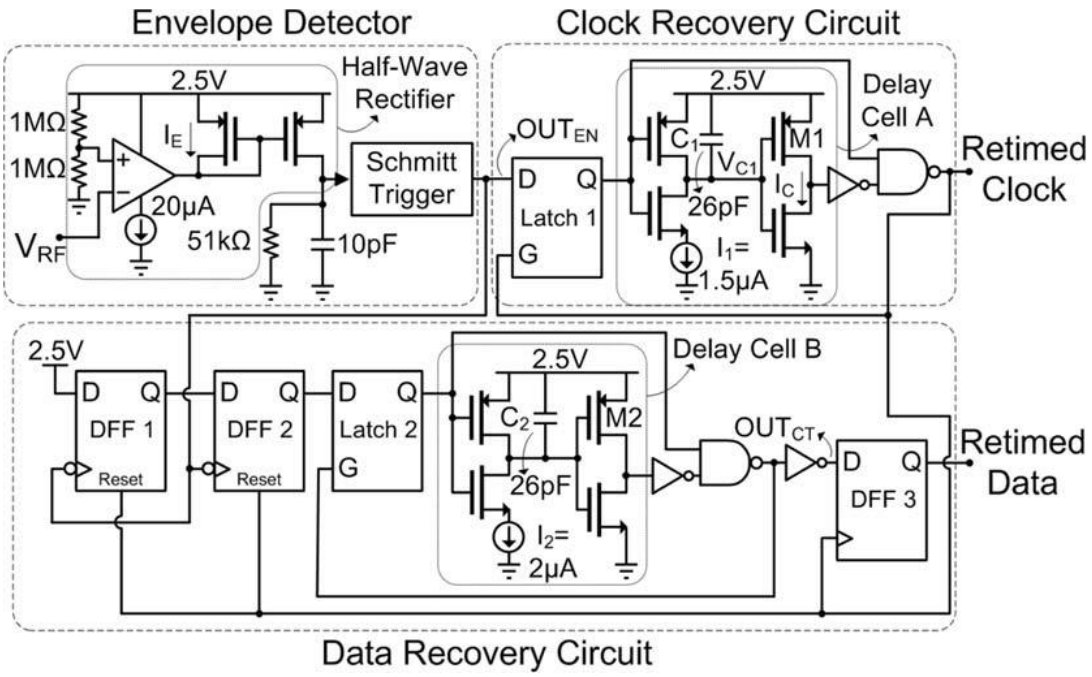


Fig.2.17. Clock/data recovery circuit in [35]

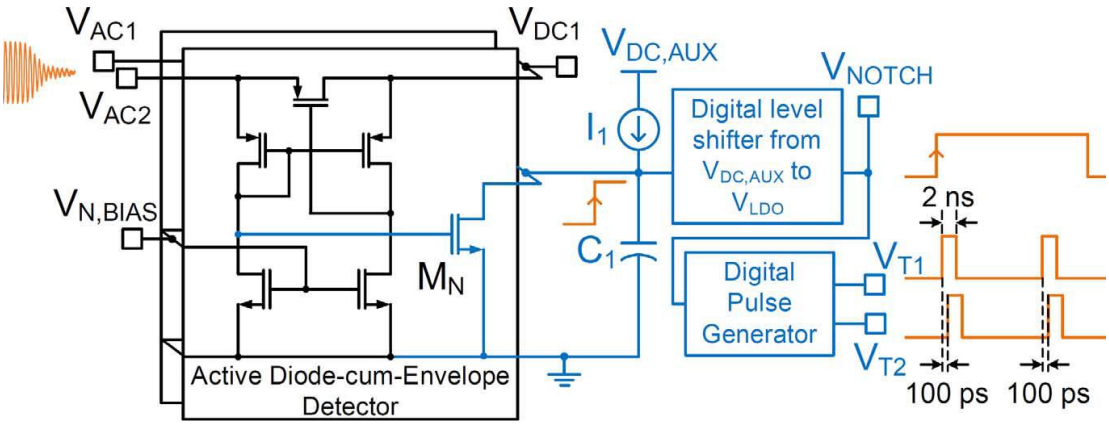


Fig.2.18. Data recovery circuit in [42]

The initial stage in most division multiplexing methods is to separate the multiplexed data. The system in Fig.2.19 is frequency division multiplexing, thus the first step is frequency division demultiplexing using a bandpass filter. The envelope detection of each dived data is the next stage [1].

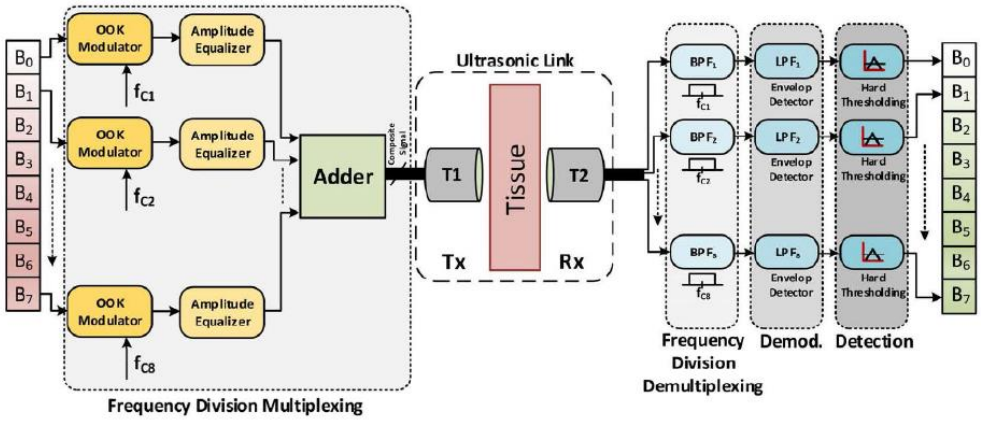


Fig.2.19. Data recovery system of [1]

## *2.4.3. Performance Measures*

To review and analyze works in a better way, certain performance measures need to be introduced and ultimately compared with similar works. Since this thesis focuses on data telemetry, important metrics for data transmission are going to be introduced in this section:

- ***Data Rate (bit rate):*** The most important metric to assess the performance of a technique is the amount of data transmitted throughout a certain period

$$Data\ Rate = \frac{Number\ of\ Bits}{\text{Time(s)}} \tag{2.2}$$

So, if a 100-bit sequence could be transmitted in a 1-millisecond period for a technique the data rate would be 100/ $(1*10^{-3}) = 10^5$ which means the data rate for this specific technique is 100 kilobits per second (Kbps).

The main importance of data rate is that the data telemetry with higher data rate could be used for more applications such as image processing that require data rates in the range of megabits per second. The main limitation of ultrasonic data telemetry is the fact that the

data rate for current methods are limited to a few hundreds of kilobits and as a result, the applications for ultrasonic data telemetry are restricted.

- ***Signal-to-Noise Ratio (SNR):*** As it could be guessed from the name of this metric, SNR represents the noise in the system at the input of the receiver as the ratio of the signal peak-to-peak to the noise peak-to-peak as it is shown in Fig.2.20 (in some works it is expressed as the ratio of average power of the received signal to the average power of noise).

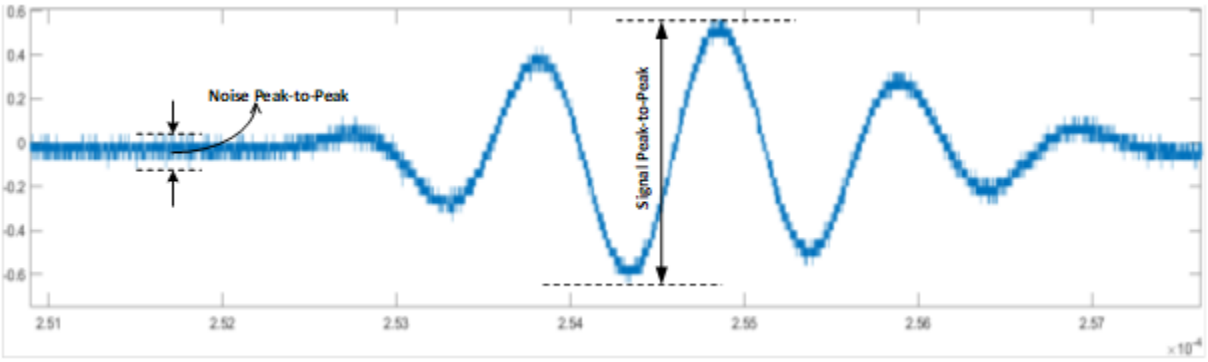


Fig.2.20. Signal peak-to-peak and noise peak-to-peak measured to calculate signal-to-noise ratio

- ***Bit Error Rate (BER):*** In digital transmission, the bit error rate is defined as the number of bits altered by noise, interference, etc. divided by the total number of transmitted bits:

$$Bit\ Error\ Rate\ (BER) = \frac{Number\ of\ Bits\ Altered}{\text{Total Number of Bits}} \tag{2.3}$$

As expected, smaller bit error rate is better and means the link is less prone to error.

# Chapter 3: The Proposed Modulation Scheme

# Chapter 3: The Proposed Modulation Scheme

One of the constraints on data rate of ultrasonic links is that, due to the limited bandwidth, the data rate is limited. The central frequency of the transducers limits the amount of data that can be transmitted between the transmitter and the receiver. This limitation is caused by the fact that in these methods, the speed of data transmission is limited by the speed of the transition between 0 and 1. As a fundamental limiting factor, the transition speed is traditionally determined by the central frequency of the transducer and causes the limited data rate in these works.

In this chapter, a novel modulation scheme is proposed which helps achieve a higher data rate of data telemetry in ultrasonic links. The proposed scheme is based on two pairs of transducers of different central frequencies, one on the transmitter side and one on the receiver side. The transducers are excited using Pulse Harmonic Modulation (PHM) proposed in [2]. The data is conveyed using temporal spacing between the excitations of the two transmitting transducers. In other words, there are two parallel ultrasonic links operating at different frequencies, and we are taking advantage of the fact that if two ultrasonic waves with different frequencies are transmitted simultaneously, they can be separated on the receiver side.

This chapter starts by the methodology of research in section 1 outlining the steps of development, analysis, and test of the proposed idea. Section 2 introduces the fundamental idea and in section 3 we implement the idea to realize a high-rate ultrasonic data telemetry link. The key advantages of the technique are investigated in section 4 and in section 5, the mathematical relationships between key parameters are analyzed to help us better understand how to increase the bit rate.

## 3.1. Methodology

The ultimate purpose of this study is to increase the data rate over the widely used ultrasonic data telemetry methods. To do this, we will present our suggested idea, which increases the data rate over the existing literature modulation schemes. At first, the general idea is introduced and analyzed using system-level blocks explaining the path from signal generation to demodulation. The details of the generation of these two signals are explained in depth.

Following that the highest achievable bit rate with our proposed idea is investigated using key parameters. Some of these parameters depend on non-idealities such as deviation of the delay between the transmitter and receiver and noise.

Subsequently, the block-level implementation of the technique is introduced which helps us have a better idea of the signal in each stage of modulation and demodulation. These non-idealities are also investigated with mathematical relationships.

Finally, the key advantages of the technique are presented and explained briefly before being investigated experimentally in the latter stages of the work.

We continue by establishing an experimental setup for the transducers that is adaptable in terms of distance, and angle. This flexibility will enable us to characterize the transducers better and in turn lead to a better return in terms of errors that may be caused by fluctuations.

One of the aspects that was mentioned in previous sections were CAD tools for acoustic wave simulation. As our focus is mainly on data transmission, those CAD tools such as COMSOL were not used in this work.

Following that, we characterize the transducers to get a better understanding of the non-idealities and other features of transmission that may vary from what datasheets and formulas predict. To do

this, the transducer will be characterized in terms of frequency, amplitude, and distance. This characterization helps us better analyze the tests and the results and the errors that may occur.

Afterwards, we test and implement a previously described technique introduced by *Keramatzadeh et al* [2]. The main reason for choosing this work is the fact that the technique presented in this work will be the basis of our proposed idea. The implementation starts with modulation of a PBRS produced sequence, modulating the sequence based on the technique and producing the signal according to the specifications of the transducer which were clarified in characterization, sending the generated signal using our transducer, receiving the signal, then demodulating the received signal to reproduce the original sequence.

Finally, we move on to designing signalling aspects of the proposed modulation scheme using MATLAB. Again, a PBRS-generated sequence is produced, it is the modulated using our proposed scheme and considering the information attained in characterization. It should be noted that this scheme requires two sets of transmitters and receivers with different central frequencies and as a result two signals are generated in accordance with them.

In the experiment side, the two modulated signals are fed into their respective transducers using arbitrary signal generated and sent through the medium. They are received using another set of transducers, spaced equally throughout the medium, and the resulting signals are shown with an oscilloscope which has the feature of capturing the received data using a USB which enables us to analyze and demodulate the signal using MATLAB.

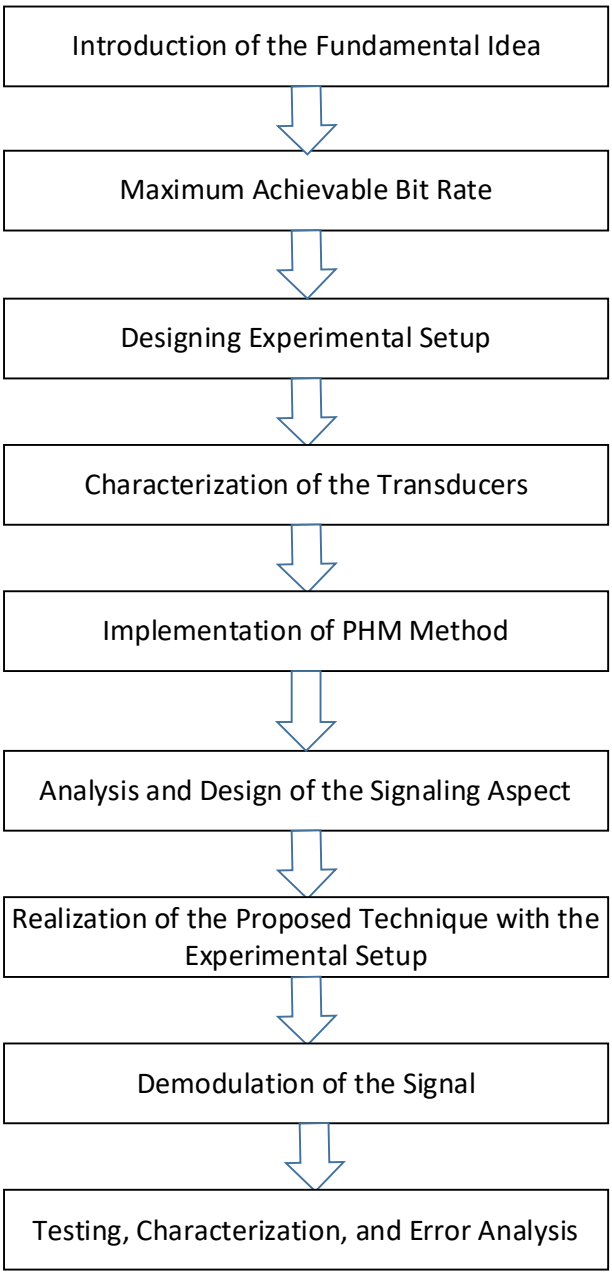


Fig.3.1. A flowchart showing the methodology

The received signal is then modulated step-by-step according to the introduced the system level blocked chart which include band-pass filtering, envelope-detection, and hard-thresholding and finally a sequence is generated.

Throughout these steps, some errors would distort the signal and cause inaccuracy in the final sequence. First, the reasons for these errors are going to be investigated.To further examine these errors, the bit error rate is benchmarked as a metric and is characterized in relationship with signal-to-noise ratio (which represents the effect of noise) and the threshold (relative to peak-to-peak voltage of the output). Because of the importance of error analysis, multiple values for these parameters are going to be tested several times to better characterize their influence on bit error rate.

At the end, the advantages, drawbacks, boundaries, and limitations of this method is going to be discussed according to our analyses and the technique is going to be compared with other works based on the important metrics which are analyzed previously with bit rate being the main one. A summary of the work is illustrated in Fig.3.1.

## 3.2. The Proposed Idea

In section 2.4, we briefly explained the pulse-harmonic modulation (PHM) scheme for the enhancement of the maximum achievable bit rate of an ultrasonic link. In the PHM scheme, the transmitting transducer generates a short tone burst in response to a well-defined excitatory-inhibitory pulse (EIP) complex as illustrated in Fig. 3.2. According to [2], for best results in terms of both the height of the tone burst envelope and its duration ($T_B$), the widths of the excitatory and inhibitory pulses ($T_E$ and $T_I$, respectively) for a transducer with a central frequency of $f_0=1/T_0$ are suggested to be both equal to half the oscillation period:

$$T_E = T_I = \frac{T_0}{2}, \tag{3.1.a}$$

their amplitudes ($A_E$ and $A_I$, respectively) need to be properly chosen, and the inter-pulse delay ($T_{IP}$) should be an integer multiple of the oscillation period:

$$T_{IP} = k.T_0 \quad (3.1.b)$$

where *k* is a positive integer number.

In the PHM method, for the transfer of a binary stream of 0s and 1s through an ultrasonic link, an on/off scheme is used (*i.e.*, a '1' is transmitted using a tone burst, and for a 0 the transmitting transducer stays off). In this approach, data telemetry bit rate is determined by the duration of the tone burst ($T_B$):

$$B.R. = \frac{1}{T_B} \quad (3.2)$$

The shortest tone burst in duration achieved for $k$ = 1 in equation 3.1.b results in the highest possible bit rate, but it is not necessarily of the highest amplitude. On the other hand, a higher tone burst peak amplitude (hence a higher *signal-to-noise ratio* (*SNR*)) is obtained by setting the *k* parameter to higher values, which is evidently at the expense of reduced bit rate. It is also a known fact that, based on fundamentals of digital communications, the lower the SNR is, the higher the *bit-error rate* (*BER*) will be. Therefore, in this approach, there is a trade-off between data telemetry bit rate on one hand, and the SNR and BER on the other hand. In general, the optimum value for the *k* parameter and therefore the maximum achievable bit rate at an acceptable BER is a function of the transducer central frequency and bandwidth. In [2], employing a transducer with central frequency of $f_0$=1MHz and a bandwidth of 200 kHz, the k parameter is chosen as k=1 to achieve a maximum bit rate of 350 kbps.

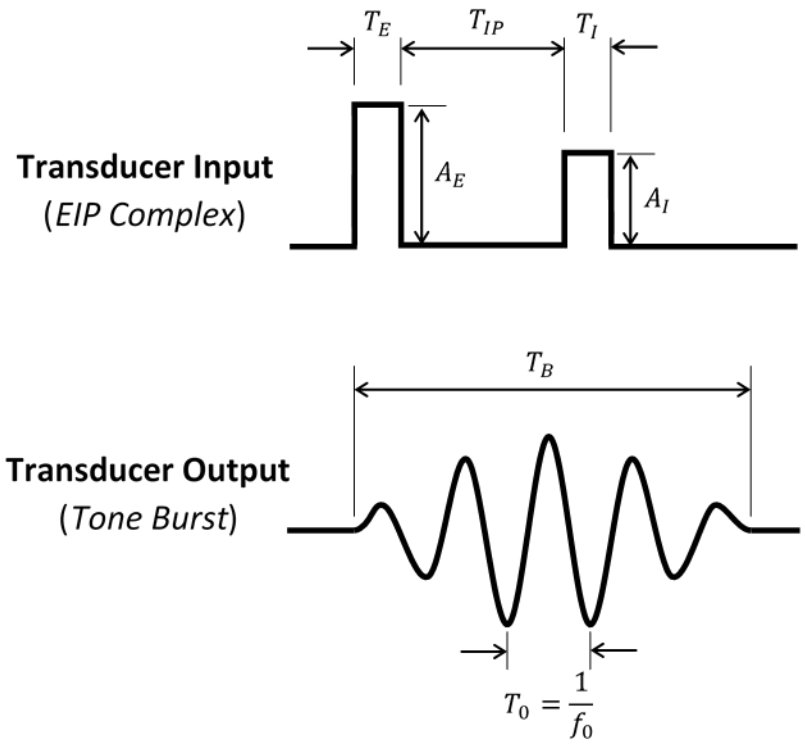


Fig.3.2 Pulse Harmonic Modulation (PHM) modulation and its resulting output [2]

In this work, it is proposed to use a dual-burst signaling for high-rate data telemetry through ultrasonic links. Classified under *isochronous pulse-based modulation* techniques, the proposed scheme takes advantage of two pairs of transducers to realize a *pulse-width modulated* (*PWM*) data telemetry link. In this scheme, transducer pairs (Tx-1&Rx-1) and (Tx-2&Rx-2) with central frequencies $f_A$ and $f_B$ are excited using EIP complexes $x_1$ and $x_2$, respectively. As illustrated in Fig. 3.3, the time shift between the excitations of Tx-A and Tx-B defines a data pulse ($x_P$), the width of which ($T_{SYM}$) conveys an *N*-bit symbol. This method is hereafter referred to as *INtervened-Timing, Enhanced-Rate Interval Modulation* (*INTERIM*) scheme.

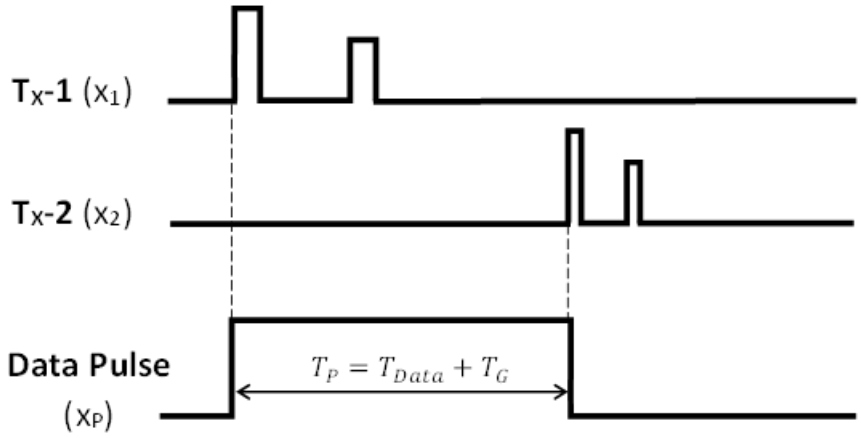


Fig.3.3. The INTERIM scheme: Defining a pulse conveying the transmitted data using the temporal spacing between two EIP excitations for transmitting transducers Tx-1 and Tx-2

The symbol time between the two complexes can be calculated by:

$$T_{Data} = D.T_{RES} \tag{3.1}$$

where $T_{RES}$ is the resolution (time step) ,and its value is determined based on the error margins (which will be discussed in Sec.3.5). D is the value of the N-bit data symbol and is calculated by:

$$D = 2^0 b_0 + 2^1 b_1 + \ldots + 2^{N-1} b_{N-1} \tag{3.2}$$

and $B = (b_{N-1} \ldots b_1 b_0)_2$ is the N-bit data symbol.

Another factor that must be taken into consideration is the guard time ($T_G$) which is the duration of the interval when D = 0. Guard time facilitates the demodulation circuits better recognize the transitions between “0” to “1” and vice versa. In other words, without guard time, $T_P$ can be so small that it prevents the amplitude from rising to a recognisable level. A guard time equaling 10% of the maximum value of $T_P$ is acceptable according to the literature [51], [52].

To conclude, two transducers are employed in this work: the TL1000KA with a central frequency of 1MHz and the A309S-SU with a central frequency of 5MHz. For the excitation of the two

transducers, the PHM approach is utilized due to its inherent advantage in terms of having a short tone burst.

All steps of the implementation of the INTERIM technique, from modulation on the transmitting side of the link to demodulation on the receiver side are shown in Fig.3.4. First, the data being transmitted is modulated in the INTERIM block, which realizes the scheme introduced in Fig. 3.3. The result is the generation of two EIP complexes for the excitation of transmitting transducers Tx-1 and Tx-2 with central frequencies *f1* and *f2*, respectively. The resulting tone bursts pass through the wireless link medium (biological tissues in real scenarios) and detected on the receiver side of the link using the receiver transducers Rx-1 and Rx-2. The receive signals are then rectified, low-pass filtered, and hard-thresholded. The result, at this point, is a pair of rectangular pulses, the rising edges of which defining the width of a pulse conveying the data. Finally, the width of the data pulse is used to retrieve the data transferred through the telemetry channel.

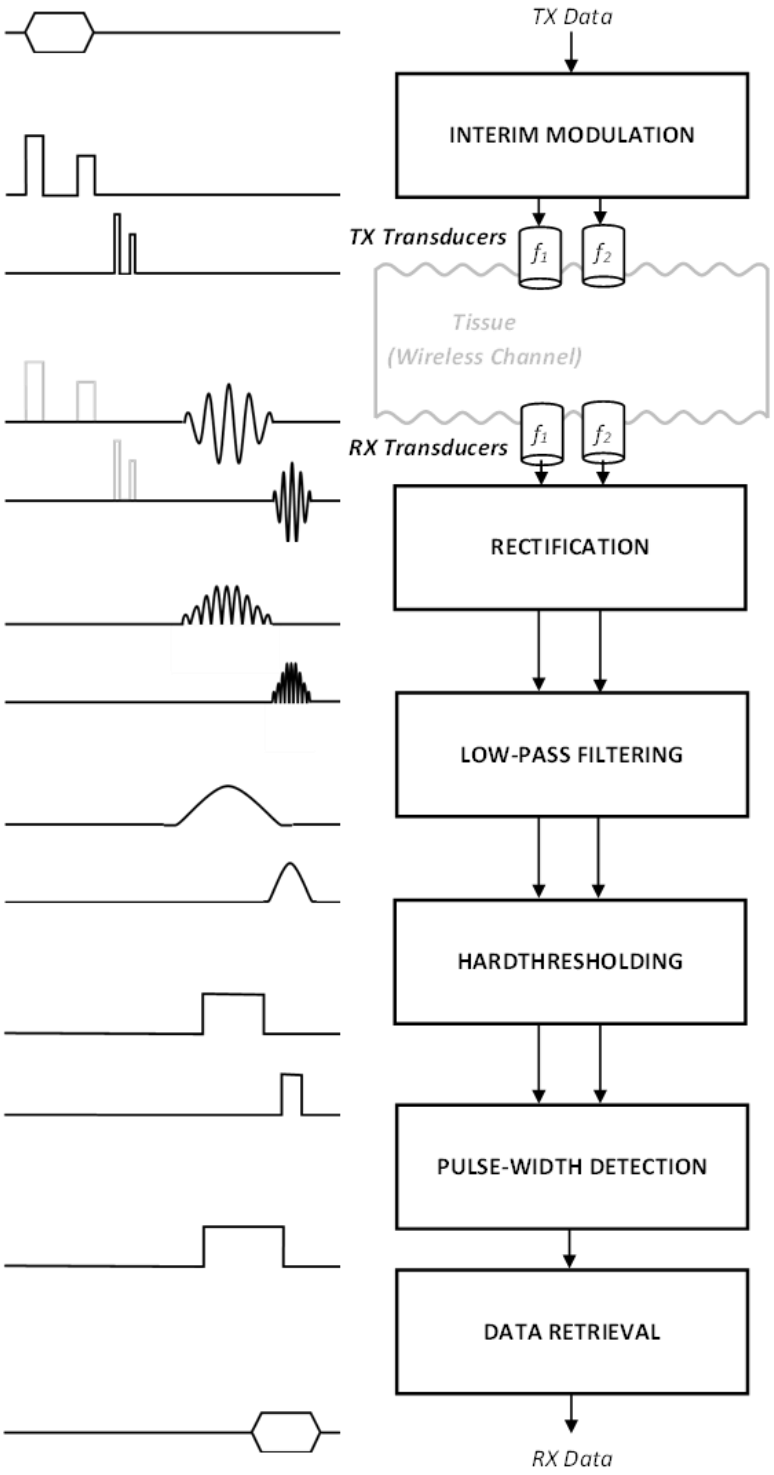


Fig.3.4. Block-level representation of the implementation of the proposed modulation scheme (INTERIM) on both sides of an ultrasonic link

## 3.3. Maximum Achievable Bit Rate

To calculate the maximum bit rate achievable with INTERIM, we use the technique in [2] called pulse harmonic modulation (PHM) as a reference point and compare the two works.

### *3.3.1. Maximum Achievable Bit Rate of PHM Method*

The maximum achievable bit rate in PHM method depends on the tone burst width ($T_B$**)** as shown in Fig.3.2. The tone burst width $T_B$ (which is the limiting factor for the bit rate) is an odd multiple (L) of half-period ($T_0/2$) and is determined by the inter-pulse delay ($T_{IP}$). To generate a 180-degree phase difference between their respective tone bursts, $T_{IP}$ must be an even multiple (M) of the half-period.

The choice of M affects the performance of the link by means of the bit rate and bit error rate. A lower value for M results in a reduced signal-to-noise ratio and hence a higher bit error rate, since it hinders the tone burst generated by the excitatory pulse from reaching its steady-state peak amplitude before being suppressed. A higher value of M results in a lower bit rate but also smaller bit error rate. As a result, there is an intrinsic trade-off between the bit rate and bit error rate that determines the spacing between the excitatory and inhibitory pulses.

For a spacing of 2 half-periods, L equals 5 which means that in theory the width of the tone burst to be 5 ($T_0/2$). But after experiment, we realized that in practice, with a spacing of 2 half-periods, L equals 7 or 9 which further decreases the bit rate in this work. The maximum achievable bit rate for PHM method is calculated by:

$$\text{Max. Bit Rate} = \frac{1}{T_B} = \frac{1}{L(\frac{T}{2})} = \frac{2f_0}{L} \tag{3.3}$$

hence, L = 5 and $f_0$ = 1 MHz result to a bit rate of 400 kbps. However, in [2] the bit rate is reported at 350 kbps to avoid inter-symbol interference.

### *3.3.2. Maximum Achievable Bit Rate of INTERIM*

Due to the more complex nature of INTERIM compared to the PHM, there are a lot of parameters such as step time and symbol time that contribute to the maximum achievable bit rate as it is shown in Fig.3.5. First, the minimum value for the step time ($T_{RES}$) should be calculated. This value depends on the variation of the delay between the transmitting transducers and their corresponding receiving transducers. The time step also depends on the signal-to-noise ratio that can cause error in recovering the transmitted symbol. Another factor that contributes to the maximum achievable bit rate is the guard time at the beginning of each symbol.

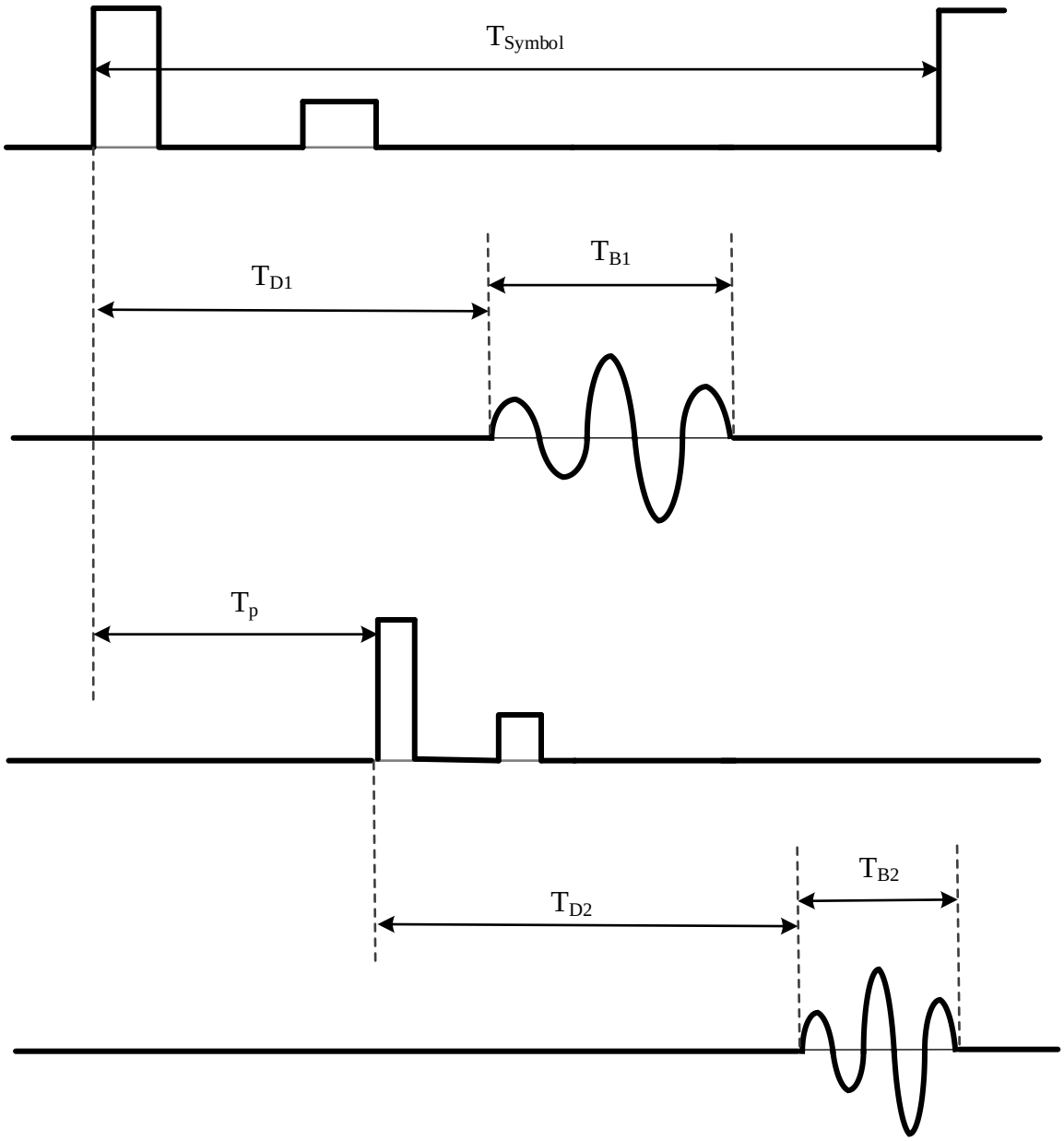


Fig.3.5. Calculating bit rate in the proposed modulation scheme

## *3.3.1. Symbol time*

Each symbol requires time for the tone burst width of each inhibitory-excitatory pulse complex ($T_{B1,2}$), the maximum spacing between the excitation of the two transmitters ($T_{P,max}$), and a guard

time ($T_G$) at the start of each symbol. The delay value does not affect the symbol time as it can be considered as latency which is of deterministic nature over the transmission. The maximum pulse interval between the two excitations allocated to the symbol can be calculated by:

$$T_{Data,\,max} = (2^N - 1)\, T_{RES} \tag{3.4.a}$$

$$T_{P,max} = T_{Data,max} + T_G \tag{3.4.b}$$

The tone burst for the first excitation can be disregarded in the symbol time calculation since it is shorter than the required time for data transmission. As a result, the symbol time can be calculated as below:

$$T_{Symbol} = T_{P,max} + T_{B2} = T_G + T_{Data,\,max} + T_{B2} \tag{3.5}$$

## *3.3.2. Step Time*

Theoretically, step time can be any small positive value but in practice multiple factors such as deviation in the delay between the transmitting transducer and the receiving transducer and the error caused by the noise in the hard-thresholding stage affect the step time.

### *3.3.2.1. Deviation of Delay*

The duration of time as the acoustic wave travels through the medium from the transmitting transducer to the receiving transducer ($T_{D1}$ and $T_{D2}$) is not constant throughout the experiment. As a result, we will design an experiment in Chapter 4 to account for the mean value and its deviation from the mean. Since $T_{D1}$ and $T_{D2}$ are not equal and $T_{D1}$ - $T_{D2}$ is of deterministic nature, the delay can be taken into consideration in the programming of the excitations. However, the delay deviation should be considered in the calculation of the step time as it impacts the timing of the

received signal which can consequently affect the recovered sequence. The delays can be written as followed:

$$T_{D1} = T_{D1,mean} \pm \epsilon_{td1} \tag{3.6}$$

$$T_{D2} = T_{D2,mean} \pm \epsilon_{td2} \tag{3.7}$$

where $\epsilon_{td1}$ $and$ $\epsilon_{td2}$ are the deviations. If we denote the approximation error for the post-processing as $\epsilon_{p-p}$, the step time could be calculated as a function of these three parameters:

$$T_{RES} = f(\epsilon_{td1}, \epsilon_{td2}, \epsilon_{p-p}) \tag{3.8}$$

There is a trade-off in choosing an optimum step time as a higher value result in a decreased bit error rate and a smaller value result in an increased bit rate. In equation (3.8), $\epsilon_{td1}$ and $\epsilon_{td2}$ are values calculated later experimentally but $\epsilon_{p-p}$ is calculated analytically. With the values achieved analytically and experimentally a $T_{RES}$ of 0.1μs is selected for the experiment.

#### *3.3.2.2. Hard-Thresholding Approximation Error*

One of the important non-idealities that affects the output is the impact of noise on the signal amplitude at the point of threshold. As explained previously, the proposed modulation is based on the timing of the signals and any variation in the timing can cause a higher error rate in the output. As it is presented in Fig.3.6, a noisy signal can result in an inaccurate timing for the hard-threshold output which is subsequently fed into the flop-flop.

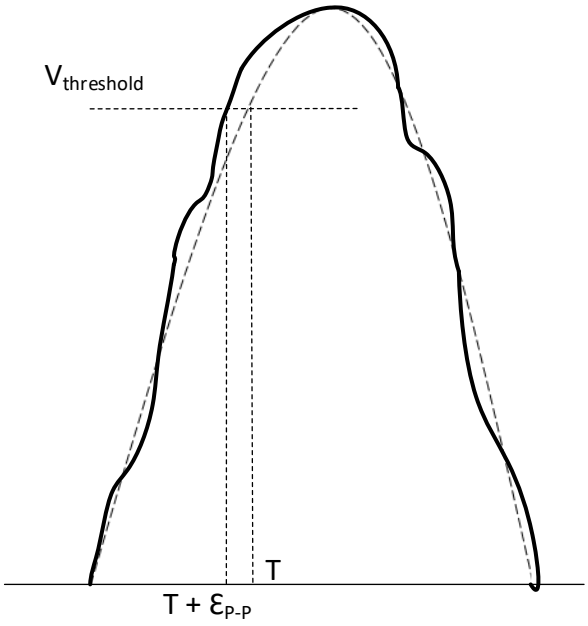


Fig.3.6. Effect of Noise on Hard-Thresholding

To estimate this error, we can use Fig.3.7 which presents an approximation of the noise effect in the timing of the hard-threshold output.

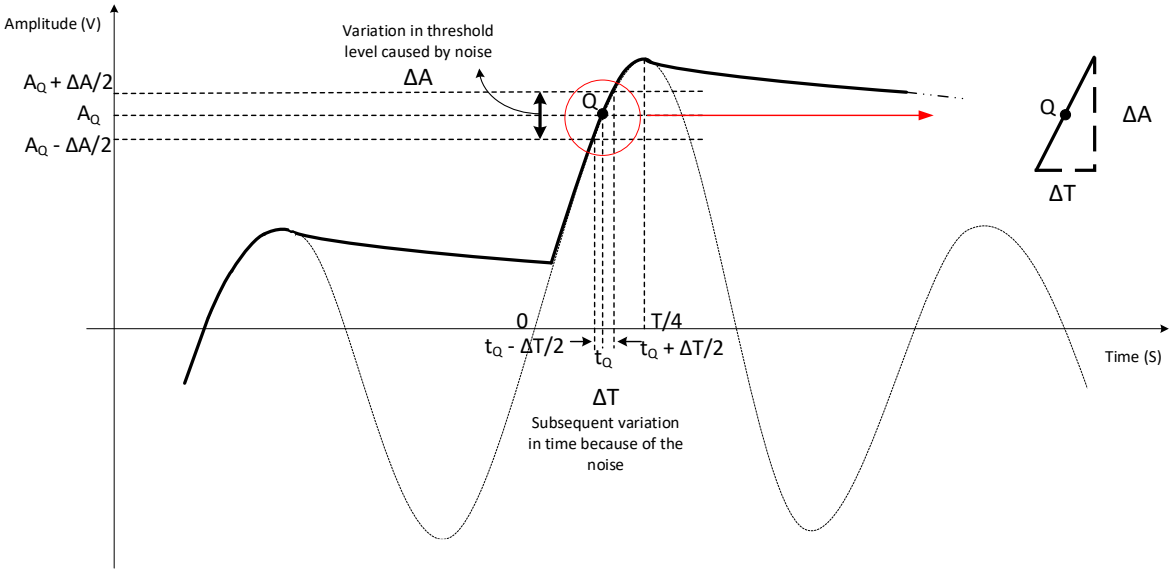


Fig.3.7. Calculation of hard-thresholding approximation error

The main source of error is the fluctuation in the timing resulting from the noise at the point of threshold. This variance in the timing can be calculated by the value of SNR and the ratio of threshold voltage to peak voltage. Certain assumptions have been made to simplify the calculation of the timing variances. First, the value of the SNR is selected to be 20 according to the experimental results. In terms of the threshold level, any value between 50% and 95% of peak voltage (since it must be greater than the first peak) is suitable.

As the fluctuations caused by noise are small relative to the peak voltage (for an SNR of 20 it is 0.05 times smaller), the sine wave can be assumed as a straight line at the point of threshold.

Assuming a threshold level of 0.8 $V_P$ and a frequency of 1MHz:

$$\Delta V = 0.05\ V_P \tag{3.9}$$

$$\text{Slope at } Q = \Delta A/\Delta T = \cos(\arcsin(0.8)) = 0.6 \tag{3.10}$$

$$\Delta T/(T/4) = \frac{1}{slope}\Delta V/V_P = \frac{1}{0.6}0.05 = 0.083 \tag{3.11}$$

$$\Delta T = (250ns)(0.083) = 20.75ns \tag{3.12}$$

### *3.3.3. Bit Rate*

The bit rate of this modulation depends on the number of bits in each symbol (N) and the time needed for the symbol ($T_{Symbol}$):

$$\text{Bit Rate} = \frac{N}{T_{Symbol}} \tag{3.13}$$

In summary, the bit rate can be written as:

$$\text{Bit Rate} = \frac{N}{T_G + (2^n - 1)\mathrm{T_{RES}} + \mathrm{T}_{B2}} \tag{3.14}$$

As it is shown, the effect of tone burst is significantly smaller than PHM modulation. This is since $T_{B2}$ is much smaller than symbol time. Assuming N = 7 , $T_{RES}$ = 0.1 µs, $T_{b2}$ = 0.5 µs, and $T_G$ =1.3 µs, the bit rate becomes 500 kbps which is a significant improvement from the previous work.

## 3.4. Block-Level Implementation

One of the key attributes of INTERIM is the relative simplicity it offers in terms of implementation. As it is presented in Fig.3.8, all the stages of modulation and demodulation of this technique can be executed using common blocks such as band-pass filter and serial-parallel convertor.

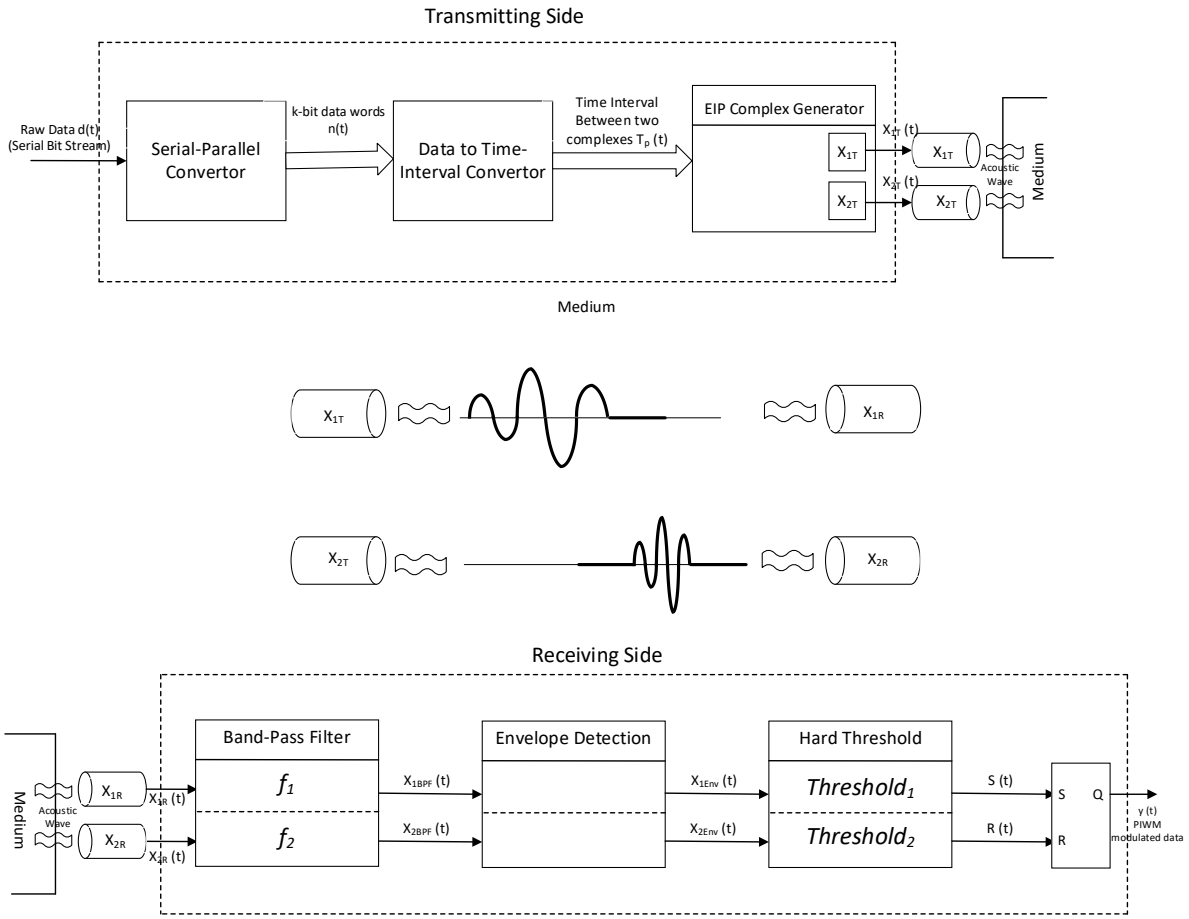


Fig.3.8. The block level review of the transmitting and receiving side of the system

# 3.5. Key Advantages

In this section, some of the key advantages of INTERIM technique are investigated. These advantages include different aspects of data telemetry such as the data rate, circuitry, and insensitivity to noise and other unwanted phenomena.

## *3.5.1. Significant Increase in Data Rate*

As it was explained in Chapter 2, the main constraint of ultrasonic data telemetry is its limited data rate. The fact that we have achieved a data rate of 500 kbps which is a significant improvement in comparison to other similar works can unlock many applications for this field.

### *3.5.2. Simple Circuit Implementation*

Given that the technique's goal is to be applied on an implant in the human body, the size of the circuitry is critical. As explained in section 3.3, one important aspect of this technique is the simplicity of its circuitry which results in small chip size as demonstrated in Fig.3.8.

### *3.5.3. Control over the Timing of the Data*

One of the drawbacks of the modulation scheme proposed in [2] is the lack of control over the timing of the data pulse complexes. This work provides control over the timing by adjusting the two transmitted signals according to the data that is being transmitted.

### *3.5.4. Power-Efficient Data Transfer*

In PHM modulation, each "1" bit requires an inhibitory-excitatory pulse complex (as shown in Figs 3.2 and 3.3). In INTERIM, however, only two PHM complexes are sent for each symbol decreasing the required power to transmit each bit. Assuming a period of $T_0$ for a transducer in PHM, the power per bit can be calculated as followed:

$$P_b = 1/2 \int_{T_B} v_{TX}(t)\, dt \qquad (3.15.a)$$

where (1/2) factor is because no pulse is transmitted for a "0" bit, and thus an average of "0" and "1" can be used. According to Fig.3.2, equation (3.15.a) becomes:

$$P_b = 1/2\ (\ A_E T_E + A_I T_I\ ) = ¼\ f_0\ (A_E + A_I) \qquad (3.15.b)$$

For INTERIM the power per bit is:

$$P_b = \frac{1}{N} \int_{T_B} \left( v_{TXA}(t) + v_{TXB}(t) \right) dt \qquad (3.16.a)$$

where N is the number of bits in a symbol and the period for a 5 MHz transducer is a fifth of a 1 MHz transducer. Likewise, equation (3.16.a) can be written as:

$$P_b = \frac{1}{N} \left( A_{EA} T_{EA} + A_{IA} T_{IA} + A_{EB} T_{EB} + A_{IB} T_{IB} \right) = \frac{1}{2N} \left( \frac{A_{EA}}{f_{01}} + \frac{A_{IA}}{f_{01}} + \frac{A_{EB}}{f_{02}} + \frac{A_{IB}}{f_{02}} \right) \qquad (3.16.b)$$

when N = 7 which is what we have chosen for this work the power consumption to transmit each bit in INTERIM could be as low as a third of PHM.

# Chapter 4: Experimental Results

# Chapter 4: Experimental Results

This chapter starts with introducing the experimental setup and the characterization of the TL1000KA transducer (the characterization was done for both transducers but the TL1000KA transducer is mentioned as the process is the same for A309S-SU transducer). The next step is the implementation of [2] as it is the base for our proposed idea. Finally, the INTERIM method is implemented, and results are illustrated.

## 4.1. The Experimental Setup

As stated in Chapter 3, the purpose of the proposed ultrasonic data telemetry approach is the transfer of digital data through living tissues. Therefore, simulation of the proposed technique in the case of living tissues as the communication channel will be a necessary step of the work. The most important properties for the link are the acoustic properties of the channel as well as attributes of the acoustic wave and the transducers used. Given that the main goal of this setup is data transfer rather than power transmission, the medium selection becomes easier. This is because impedance matching, attenuation, and other variables have a greater effect on power efficiency, which is not our primary concern.

According to table 2, water has enough similarities with different soft tissues in the human body in terms of density, sound velocity and acoustic radiation impedance. The sole distinction is in the attenuation coefficient, which remains relatively comparable in terms of its frequency dependency, which is the main point of concern.

The next step is the actual setup in which the transducers are supposed to function. Many factors should be considered in the design of the setup. These factors include (but are not limited to) the adjustability of the distance and alignment between the transmitter and receiver transducers, center

frequency of the transducers, the medium for the transfer of the acoustic waves, and the possibility of trying different excitations and signaling for the generation of ultrasound signals.

The reason for the emphasis on distance adjustability and alignment of the transducers is the fact that the target application of this experiment is for communicating with the biomedical implants that are embedded in the human body. These transducers are also subject to inevitable displacements because of patient's movement. Thus, the ability to test our link with different distances and misalignments is of critical importance.

Based on the above considerations, an ultrasonic link setup was built, which is equipped with a simple positioning system for the transmitter and receiver transducers. As shown in Fig.4.1, the setup has been designed using a liquid tank, metal rods, and flexible connectors and holders for the transducers.

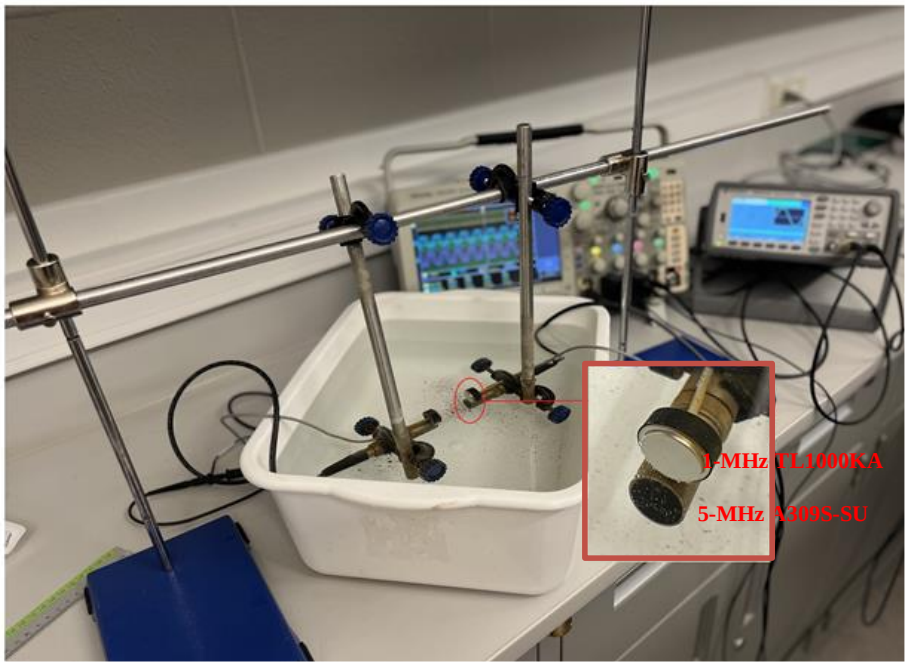


Fig.4.1. The setup using a positioning system to adjust the angle and distance of the transducers

In this setup the 1-MHz TL1000KA transducers are mounted on top of the 5-MHz A309-SU transducers with a center-to-center distance of 17 cm as is demonstrated in Fig.4.2. The distance between the transmitting and receiving transducers is adjustable between 0 to 20 cm.

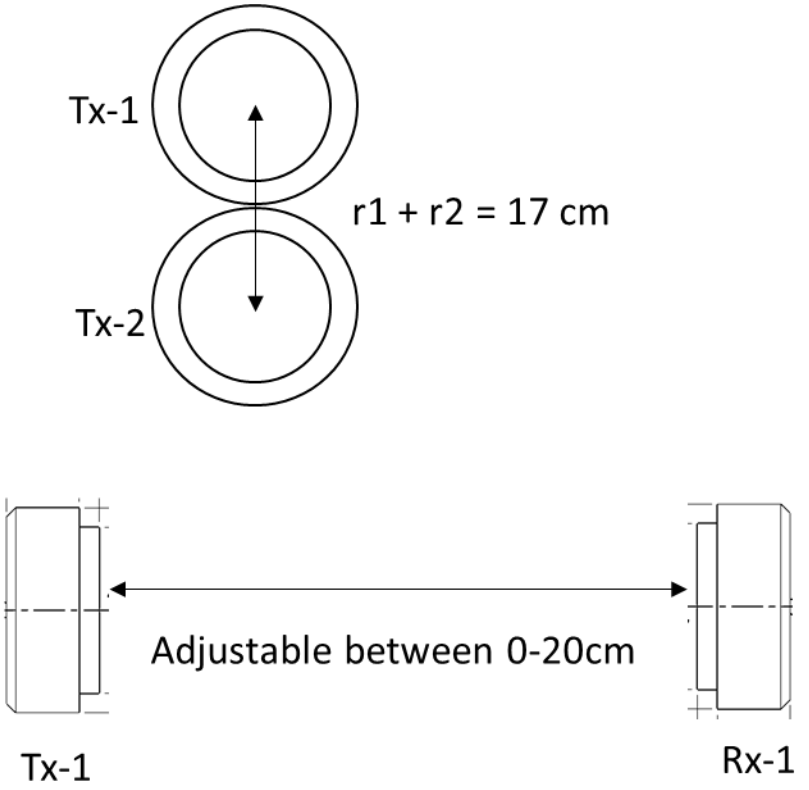


Fig.4.2. Transducer placement

In summary, what the process is for the modulation and demodulation of the signal can be seen in Fig 4.3. The process starts by generating the INTERIM modulated data and generating the corresponding signal using Keysight 33500B Waveform Generator. The generated data is given to the waveform generator using its USB connection. The signal is then fed into the two transmitting transducers and received by the two receiving transducers through the medium (water). The received signal is captured by the Tektronix MDO3024 Oscilloscope. The captured data is taken

back to the MATLAB for post-processing and demodulation using the oscilloscope USB connection.

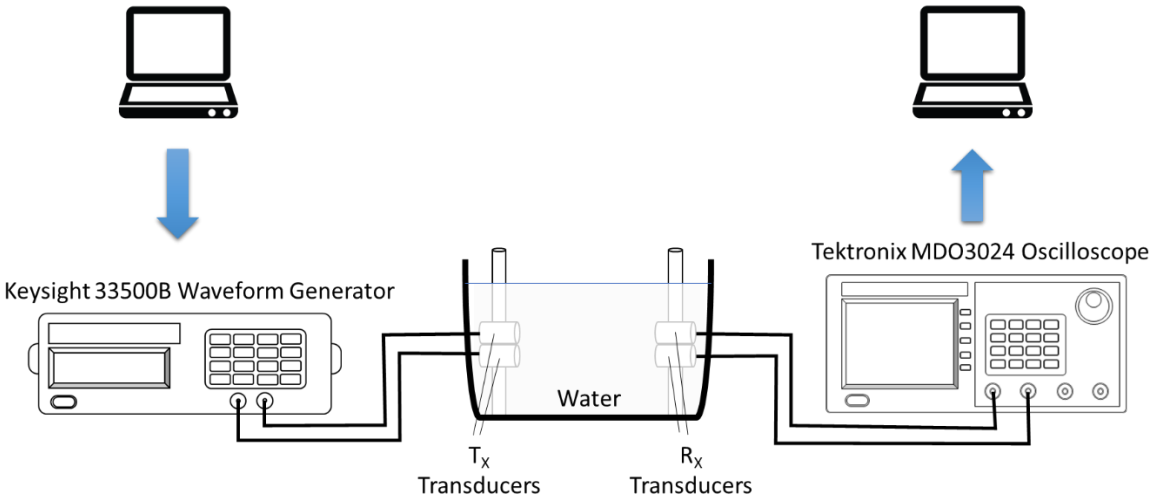


Fig.4.3. The equipment and the process of modulation and demodulation used in INTERIM

# 4.2. Transducer Characterization

In this section, the 1-MHz TL1000KA transducer and the link are characterized. To investigate the relationship between frequency and attenuation, different frequencies are tested, and the corresponding attenuation-frequency relationship is plotted. The same approach is carried out to investigate the attenuation-frequency relationship in pulse waves. The next step is to explore the effect of transducers' distance on attenuation.

## *4.2.1. Frequency Characterization*

The central frequency for TL1000KA transducer is 1MHz and the distance between transducers is 3cm. The Tektronix MDO3104 Digital Storage Oscilloscope is used for complete measurement of frequency, amplitude, phase, etc. in real-time. As shown in Fig.4.4, the input waveform is demonstrated as channel 1 (blue) and the output as channel 2 (green).

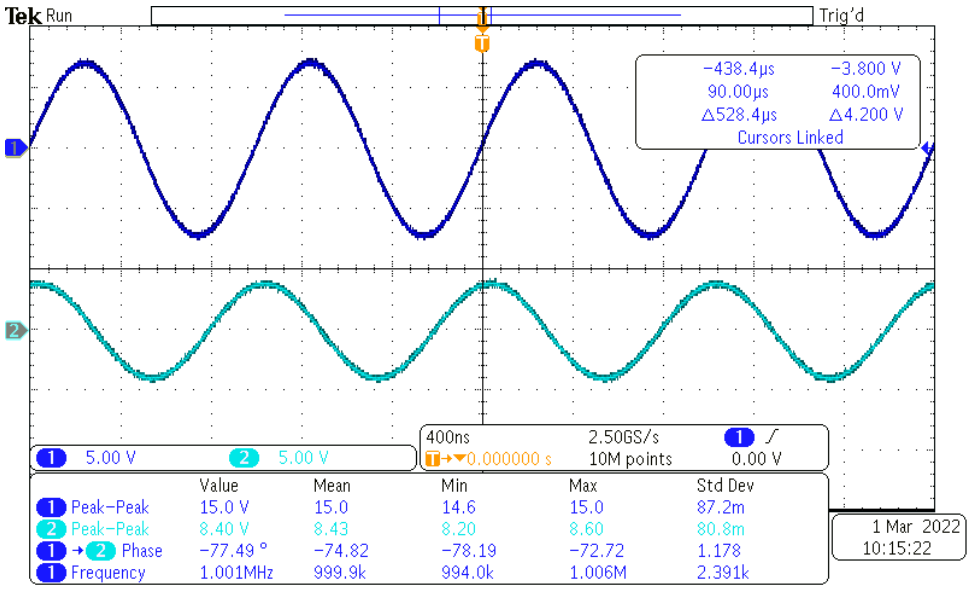


Fig.4.4. Input and output waveform and their measurements at 3cm distance and 1MHz of the 1-MHz TL1000KA

The output peak-to-peak declines as we move toward higher and lower frequencies, but this reduction is not linear.

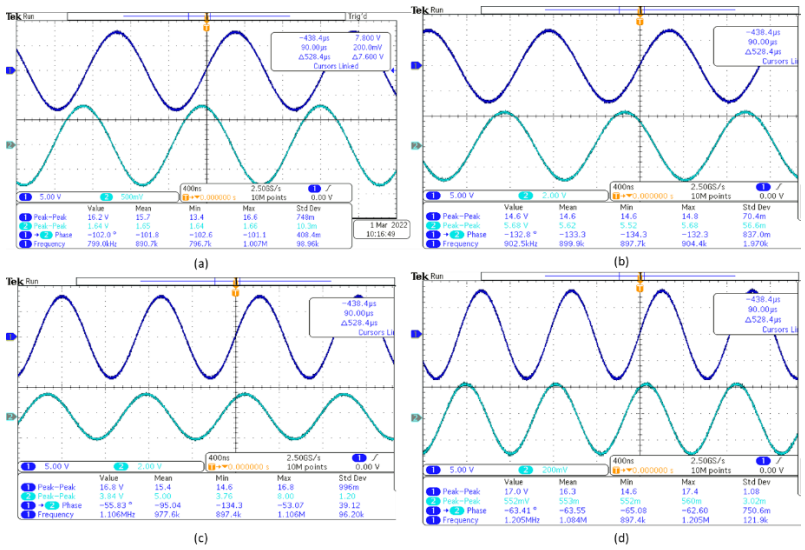


Fig.4.5. Frequency characterization of the 1-MHz TL1000KA: Input and output waveform and their measurements at 3cm distance and (a) 0.8 MHz, (b) 0.9 MHz, (c) 1.1MHz, and (d) 1.2MHz

As demonstrated in Fig.4.5, the output Peak-Peak voltage drops on either side of 1MHz transmission frequency, but the drop is not symmetrical. The frequency-attenuation relationship is represented in Fig.4.6.

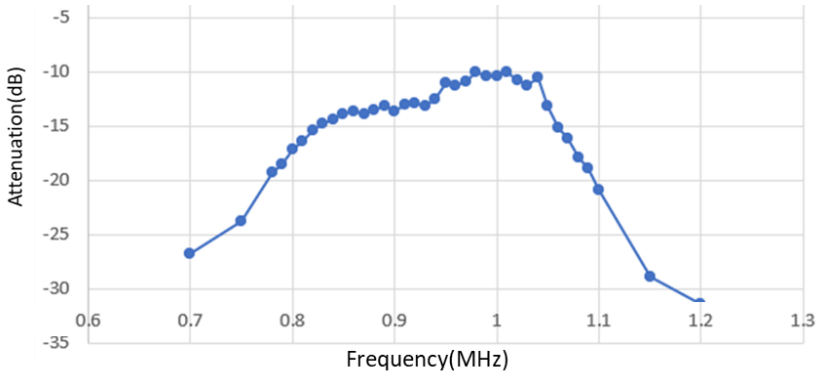


Fig.4.6. Frequency characterization of the 1-MHz TL1000KA

As shown in Fig.4.6, the transducer acts as a passband filter which operates around 1MHz central frequency and drops more steeply at the values higher than 1MHz.

### *4.2.2. Duty Cycle Characterization (Pulse)*

The duty cycle of the signal is another factor in pulse-based modulation. This factor becomes important as most pulse coding schemes contain pulses with various time differences between consecutive pulses. The effect of time difference becomes apparent once there is a knowledge of the transducer function with different duty cycles.

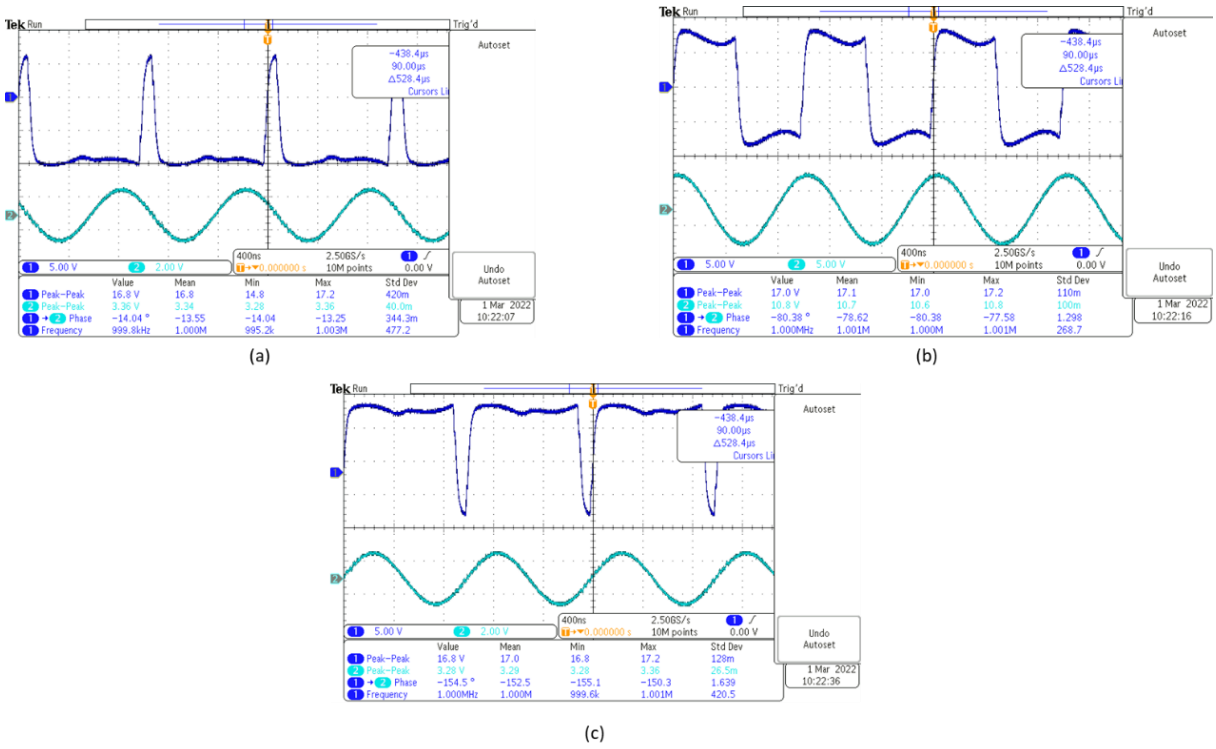


Fig.4.7. Duty cycle characterization of the 1-MHz TL1000KA at 1MHz and 3cm at (a) 10%, (b) 50%, and (c) 90%

As it is demonstrated in the Fig.4.7, the output peak-to-peak voltage is maximum at 50 percent duty cycle. The attenuation drops at higher or lower values than 50 percent, as shown in Fig.4.8.

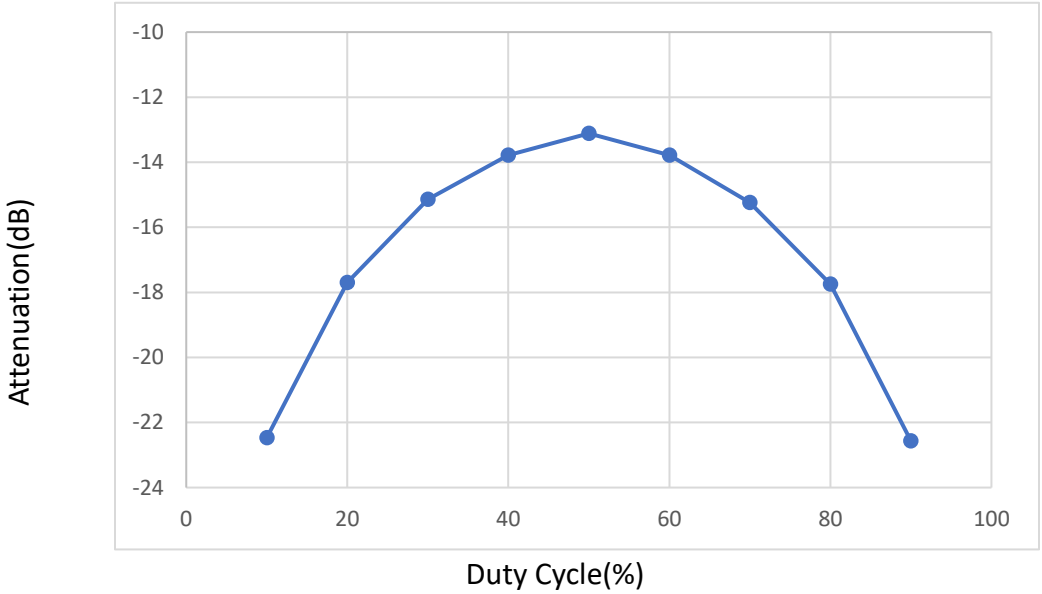


Fig.4.8. Duty cycle characterization of the 1-MHz TL1000KA

### *4.2.3. Distance Characterization*

As it was mentioned in the first chapter, the typical distance in which the transducer operates is between 3 to 20 cm. The distance is changed because of sudden body movements; thus, it is critical to characterize the distance. Two examples of this characterization are shown in Fig.4.9.

When the distance changes, two factors affect voltage attenuation. The focus distance of the transducer becomes important since there is a higher concentration of acoustic wave.

Furthermore, the attenuation increases as the distance between the two transducers rises. Because of these two factors the result is not linear.

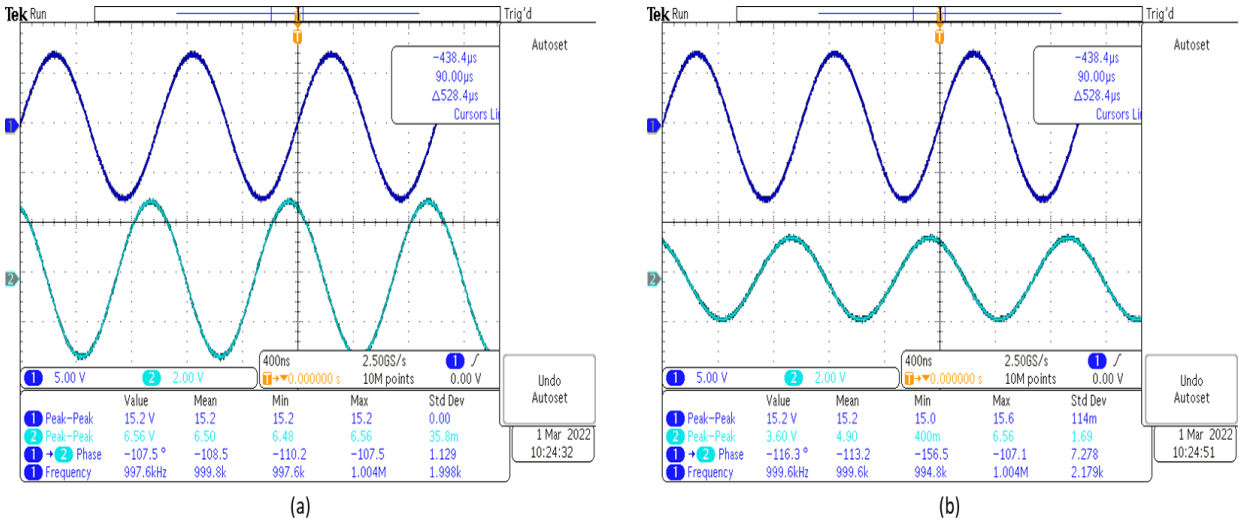


Fig.4.9. Distance characterization of the 1-MHz TL1000KA. The input and output signal at 1MHz and 1cm (a), and 18cm (b).

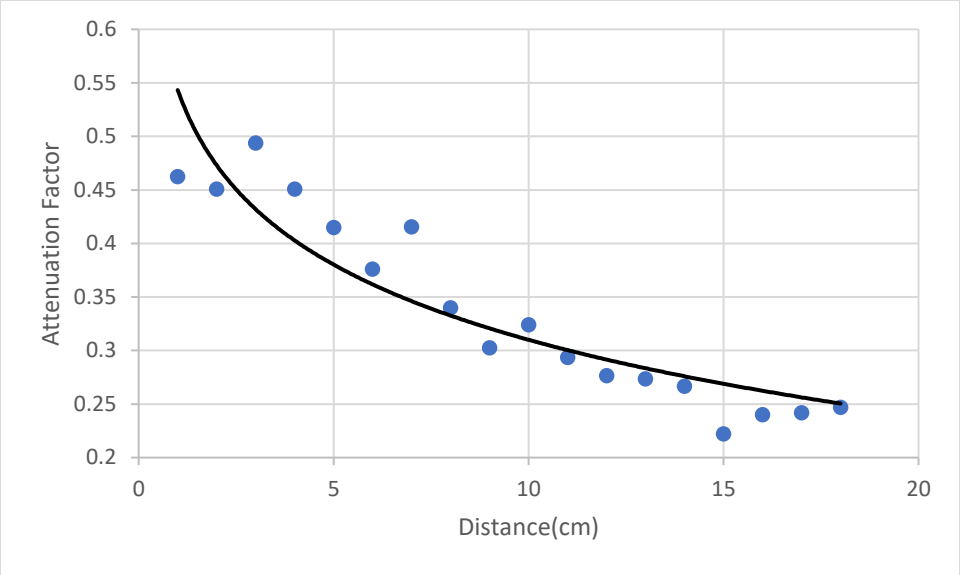


Fig.4.10. Distance characterization of the 1-MHz TL1000KA at 1MHz

As it can be noticed in Fig.4.10, the relationship between distance and attenuation follows Eq (1.10) and is not linear because the electrical to mechanical conversion is maximized at focal distance and as it is demonstrated at 3cm the attenuation is at its minimum.

## 4.3. Implementation of Pulse Harmonic Modulation (PHM)

The next step in testing the setup is using arbitrary signals as an input. These modulated sequences are generated by MATLAB. The resulting sequences are transferred to Keysight arbitrary waveform generator 33500B series to generate the signal which is then fed to the 1-MHz TL1000KA transducer. The received signal is captured from the receiving transducer using an oscilloscope and demodulated again by MATLAB. The PHM modulation in [2] is implemented in this section since it provides a basis for INTERIM modulation as explained in Chapter 3.

In this approach, the excitatory pulse ignites oscillations at the center frequency of the transducer, and the inhibitory pulse causes a second excitation with 180 degrees phase difference referenced to the ongoing oscillations of the device. Adding the inhibitory pulse with proper

timing and amplitude suppresses the transducer oscillations much earlier than when it naturally ends.

In [2], the results were presented in the form of simulation whereas, experimental studies are carried out in this thesis. Fig.4.11 shows the resulting tone bursts from the excitatory (red) and inhibitory (blue) signal separately. As it is evident in Fig.4.11, the phase difference between the tone bursts is changing throughout the duration of the tone bursts.

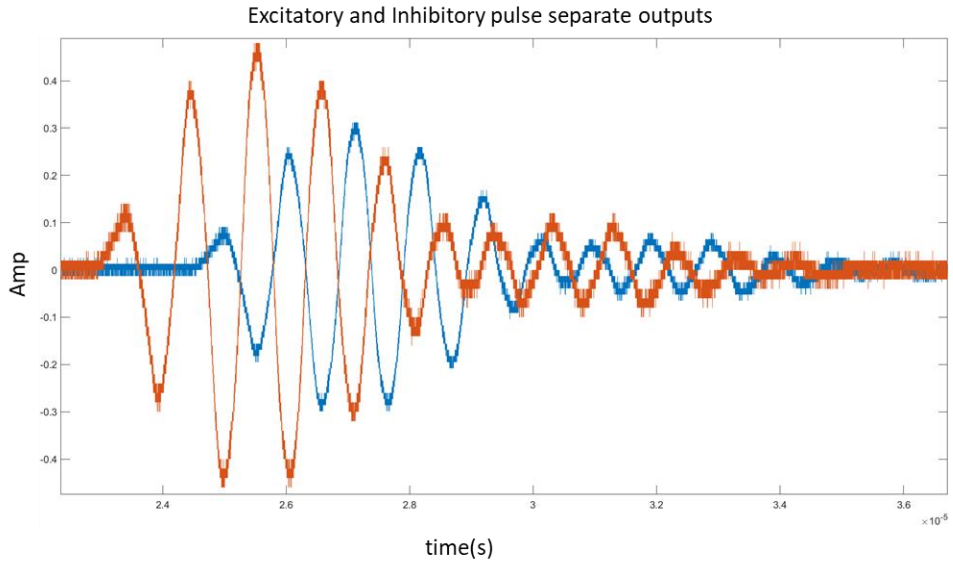


Fig.4.11. Separate output signal of excitatory (orange) and inhibitory(blue) pulses

As a result, although some of the unwanted parts of the signal has been removed but still a significant amount of the tail of the pulse remains resulting in a limited bit rate as illustrated in Fig.4.12.

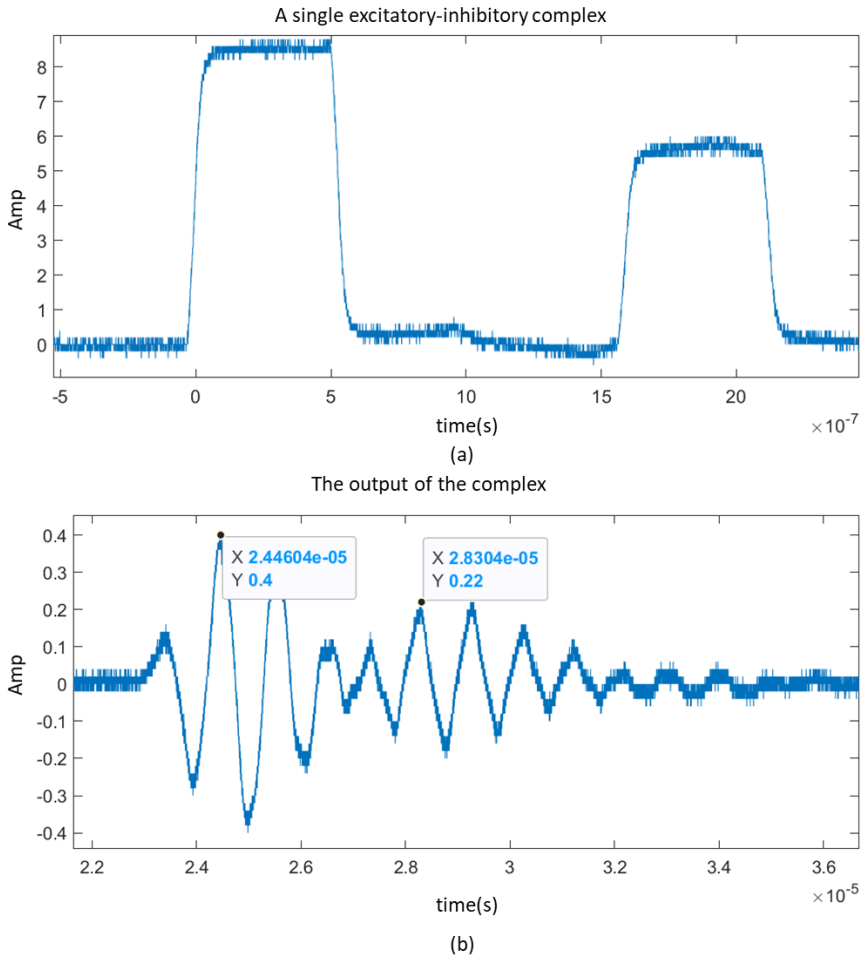


Fig. 4.12. (a) Single excitatory pulse followed by an inhibitory pulse and (b) the resulting output

The final step is the generation of a pseudo-random bit stream (PBRS) sequence, encoding the data into excitatory-inhibitory pulse pairs as shown in Fig. 4.13.

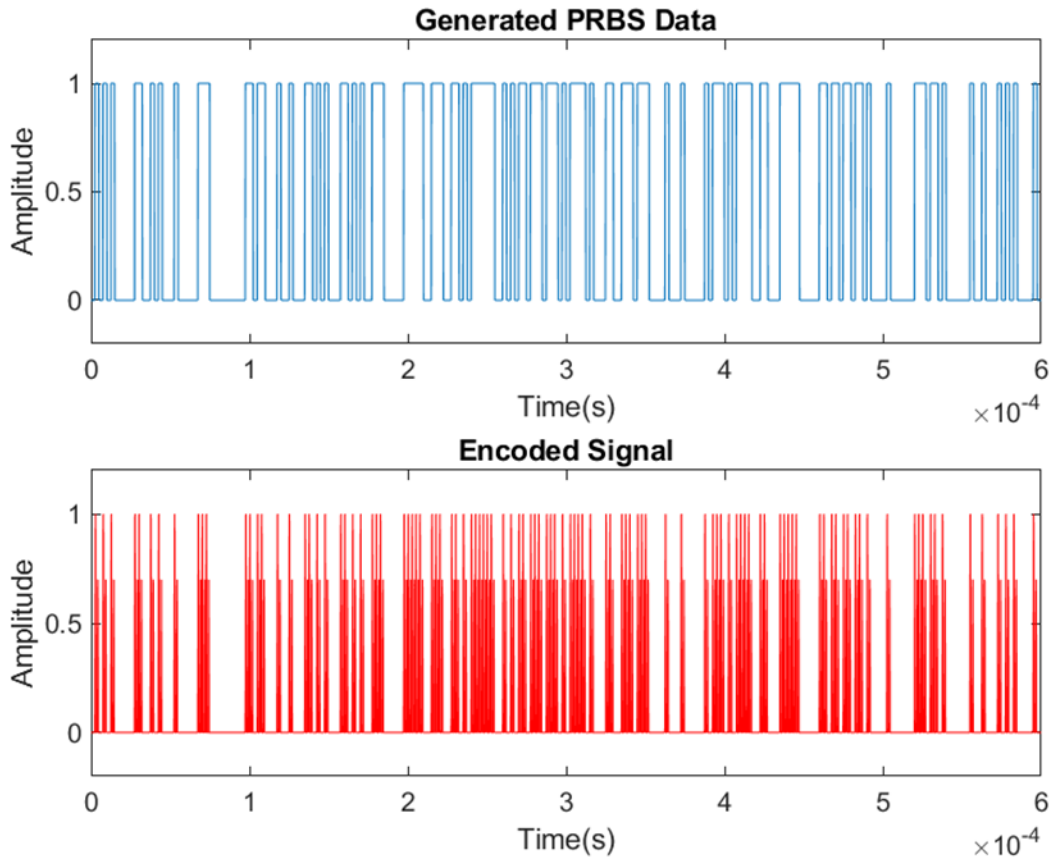


Fig. 4.13. The generated PBRS data and the encoded signal

Fig.4.14 shows the results achieved, in which the plotted signals from top to bottom are the encoded bitstream (generated using an arbitrary waveform generator), the signal captured at the receiver end, after low-pass filtering (in MATLAB), after envelope detection (in MATLAB), and finally the stream of the detected binary data (in MATLAB).

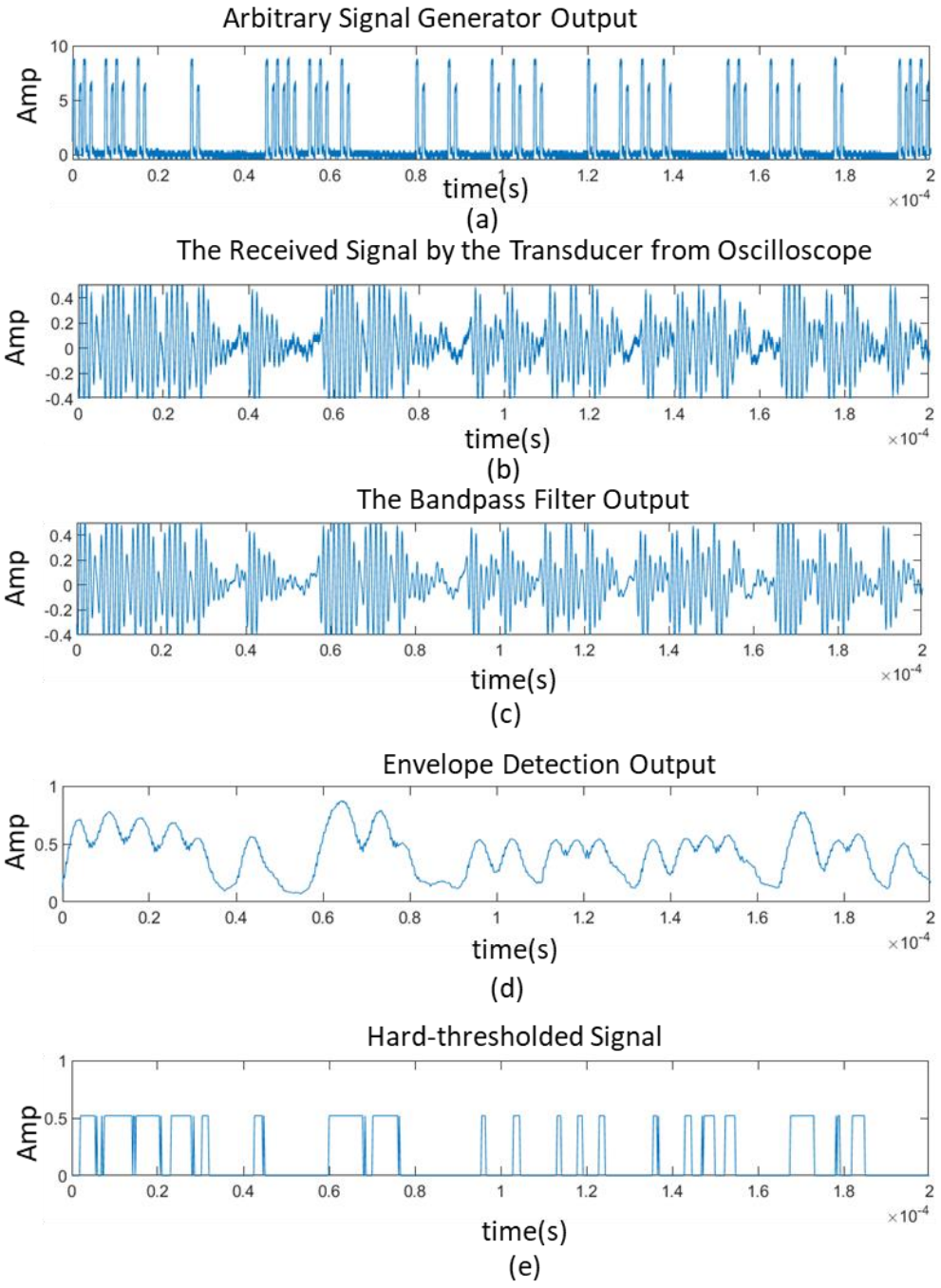


Fig.4.14. Transfer of a stream of pseudo-random binary data through the experimental setup (a)The generated signal by arbitrary signal generator (b) The received signal by the 1-MHz TL1000KA (c) low-lass filtered signal (d) envelope detected signal (e) hard-thresholded signal

## 4.4. Propagation Delay

The propagation delay and its deviation play a major part in INTERIM modulation. As explained in section 3.3, the delay deviation is a major factor in choosing the step time ($T_{Res}$). In this section, an experimental study is carried out to determine the delay and the corresponding variance.

To do so, a periodic square-wave signal with a small frequency is transmitted by both transducers simultaneously. The delay between transducers in each period is measured using MATLAB. Additionally, the delay mean is used as a baseline in the programming of the INTERIM input signals for each transducer. The standard deviation is used as a factor in calculating the time step. Fig.4.15 shows the input signal and the delay for each transducer in one of the periods. This process is repeated for 30 time periods to ensure the reproducibility of the result.

The mean value and the standard deviation of the delay for the 1-MHz TL1000KA transducer are respectively 32.9µs and 0.025µs, and for the 5-MHz A309S-SU transducer are 31.7 µs and 0.001 µs. The result summary is provided in Table 3.

Table 3 Propagation Delay

| | Transducer1 (1MHz) Delay | Transducer2 (5MHz) Delay |
|---|---|---|
| **Mean** | 32.917 µs | 31.758 µs |
| **Standard Deviation** | 24.919 ns | 9.797 ns |
| **Number of Iterations** | 30 | 30 |

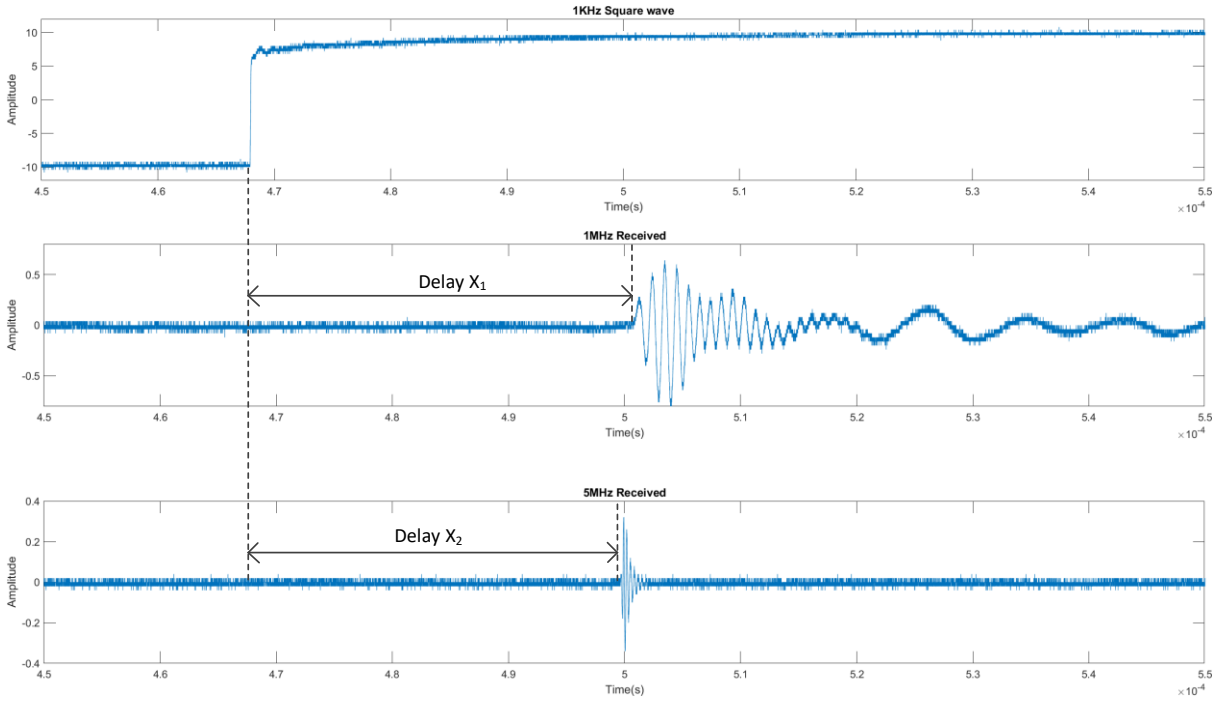


Fig.4.15. The generated 1kHz square wave to calculate the delay between the transmitter and receiver by measuring the time interval between the start of the excitation at the transmitters(top) and the receivers (middle and bottom)

# 4.5. Implementation of INTERIM Using PBRS-Generated Sequence

In this section, a PBRS generated sequence is modulated using INTERIM technique and transmitted through the link. A dataset of 140 bits consisting of 7-bit symbols is generated using MATLAB. Consequently, each symbol takes ($2^7$-1 = 127) * 0.1 µs = 12.7 µs plus the guard time ($T_G$) and the tone burst width of the secondary transducer ($T_{B2}$) (as explained it section 3.3). The 5 MHz transducer is chosen as $TX_2$ because of its shorter width. Therefore, each 7-bit data symbol is assigned a 14-µs period. The PBRS sequence consists of 20 symbols of 7 bits each and is modulated with inhibitory and excitatory pulses for both transducers. The IEP complexes for the

two transducers are spaced according to the value of the 7-bit data symbols. 3 of these 20 symbols and the resulting spacings can be observed in Fig.4.16.

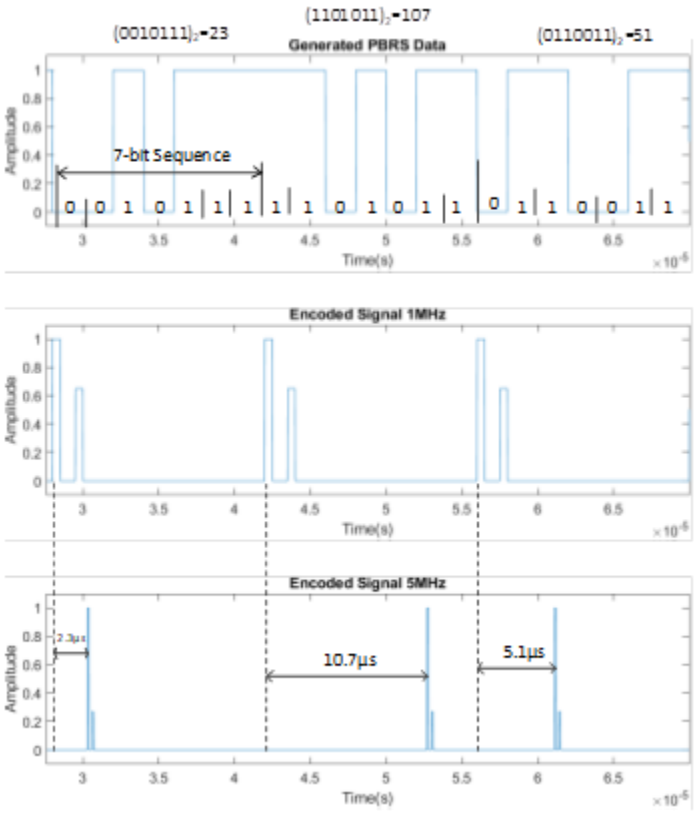


Fig.4.16. The 140-bit generated PBRS signal (top), the encoded 1MHz (middle), and 5MHz (bottom) signals with time intervals between the two encoded signals proportional to the 20 7-bit sequences

As is demonstrated in Fig.4.16, the encoded signal for the TL1000KA 1MHz transducer is evenly spread throughout the time, but the encoded signal for the A309S-SU 5MHz transducer is spaced according to the 7-bit value. For example, the first seven bits are $(0010111)_7 = 23$ implying that the gap between the first 1-MHz transducer pulse complex and the first 5-MHz transducer pulse complex should be 2.3µs.

The next step is to generate the signals corresponding to the sequence using arbitrary waveform generator. Then, these two signals are transmitted across the medium using two sets of transducers located 5cm apart in the water tank. The transmitted and received signal are shown in Fig.4.17.

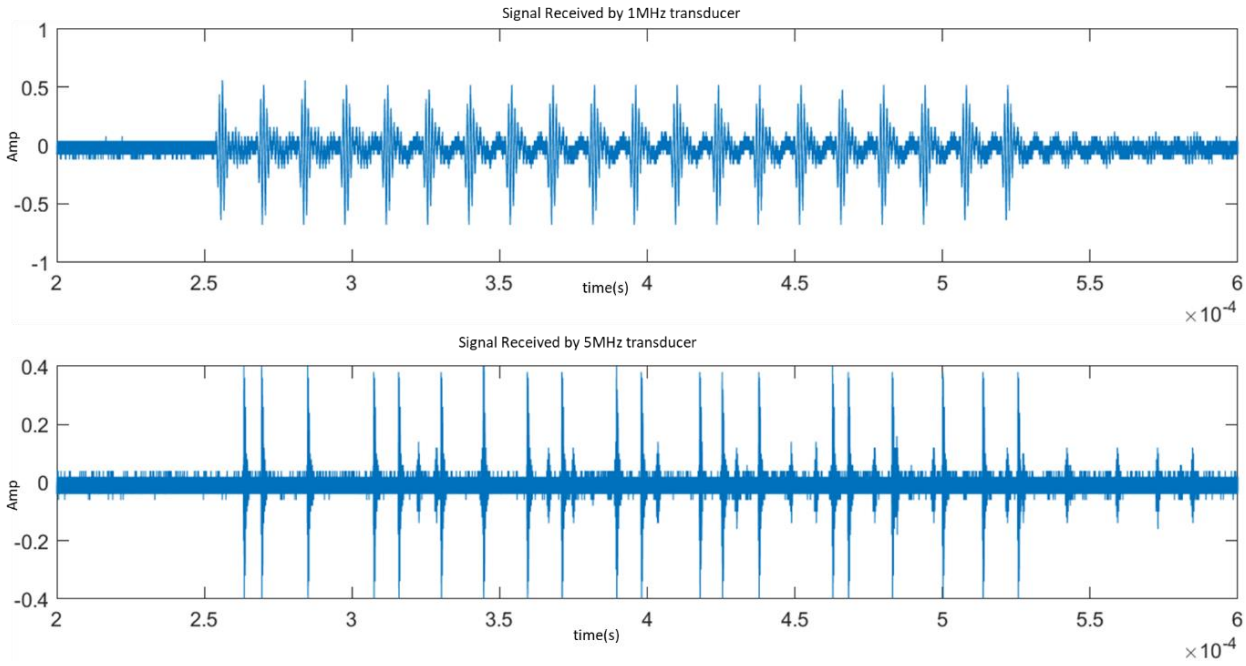


Figure 4.17. The signal received by the TL1000KA 1MHz(top) and A309S-SU 5MHz(bottom) transducers

To demodulate the signal, the first step is envelope detection, which simplifies the process of capturing individual pulses. This step introduces inaccuracy in the timing of the pulses since it affects the timing of the peak and fall of the signal, which in turn affects the spacing. Fig.4.17 illustrates the outcome of the envelop detection.

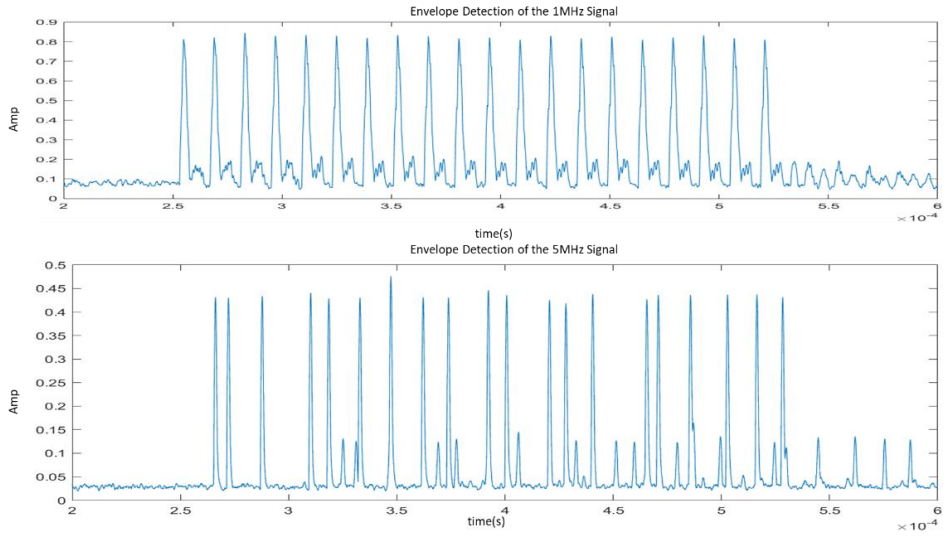


Fig.4.17. The 1MHz(top) and 5MHz(bottom) after envelope detection

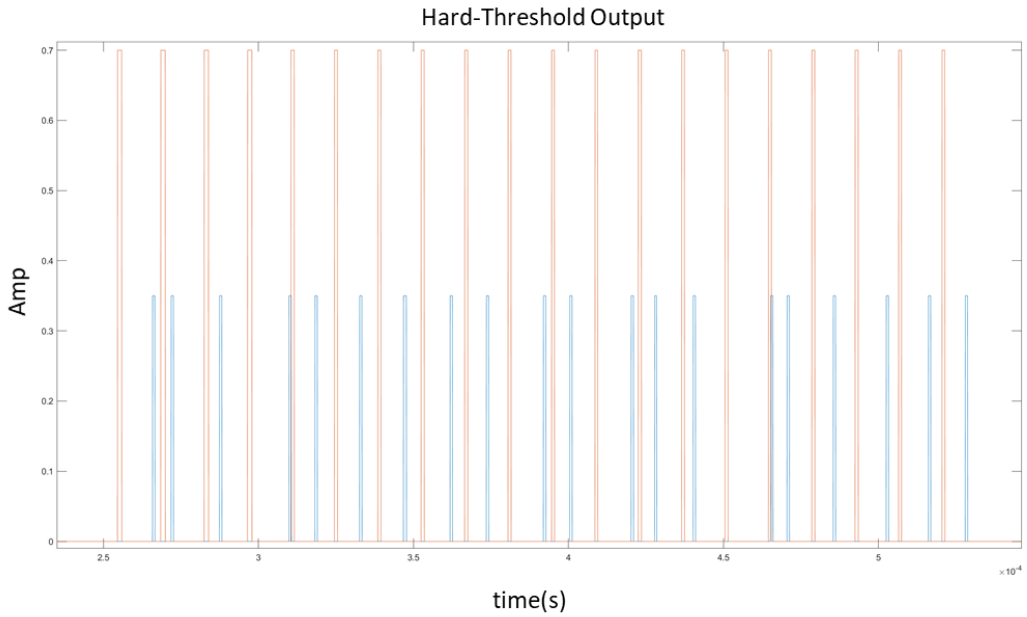


Fig.4.18. The 1MHz (Orange) and 5MHz (blue) generated pulses acting as a set and reset that could then be fed to an RS-flip flop

Next, the pulse trains are fed into the set and reset input of an RS flip-flop to generate the time spacing corresponding to each symbol. As shown in Fig.4.19, there are 20 generated pulses corresponding to the 20 7-bit original sequences.

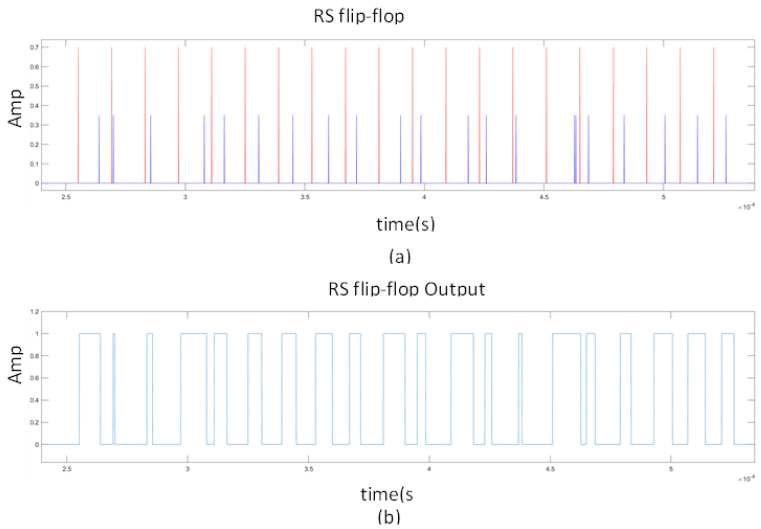


Fig.4.19. (a) The RS flip-flip input (red as input set and blue as reset), and (b) RS flip-flop output

Finally, the flip-flop output is connected to an integrator circuit to produce recovered symbols. Fig.4.20 illustrates the recovered 140-bit sequence.

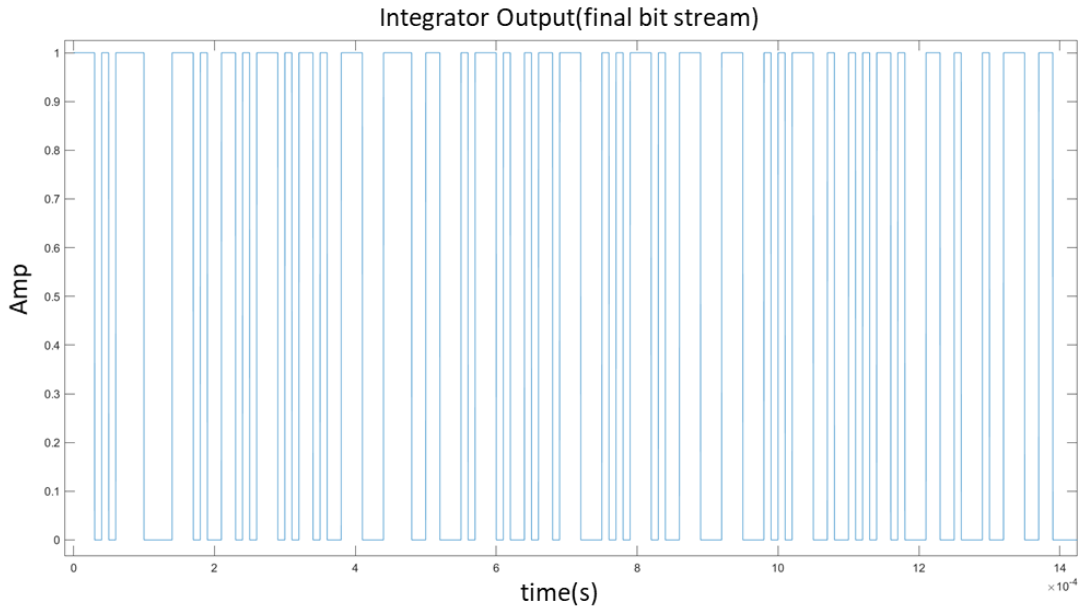


Fig.4.20. The result of demodulation. The 140 bits decoded from the initial sequence

The difference between the transmitted and received time intervals are calculated and bit error rate is determined accordingly which results in a BER of 1.4% with a 17.5 SNR. A summary of all the stages is shown in Fig.4.21, with the three 7-bit data symbols introduced at the beginning of this section.

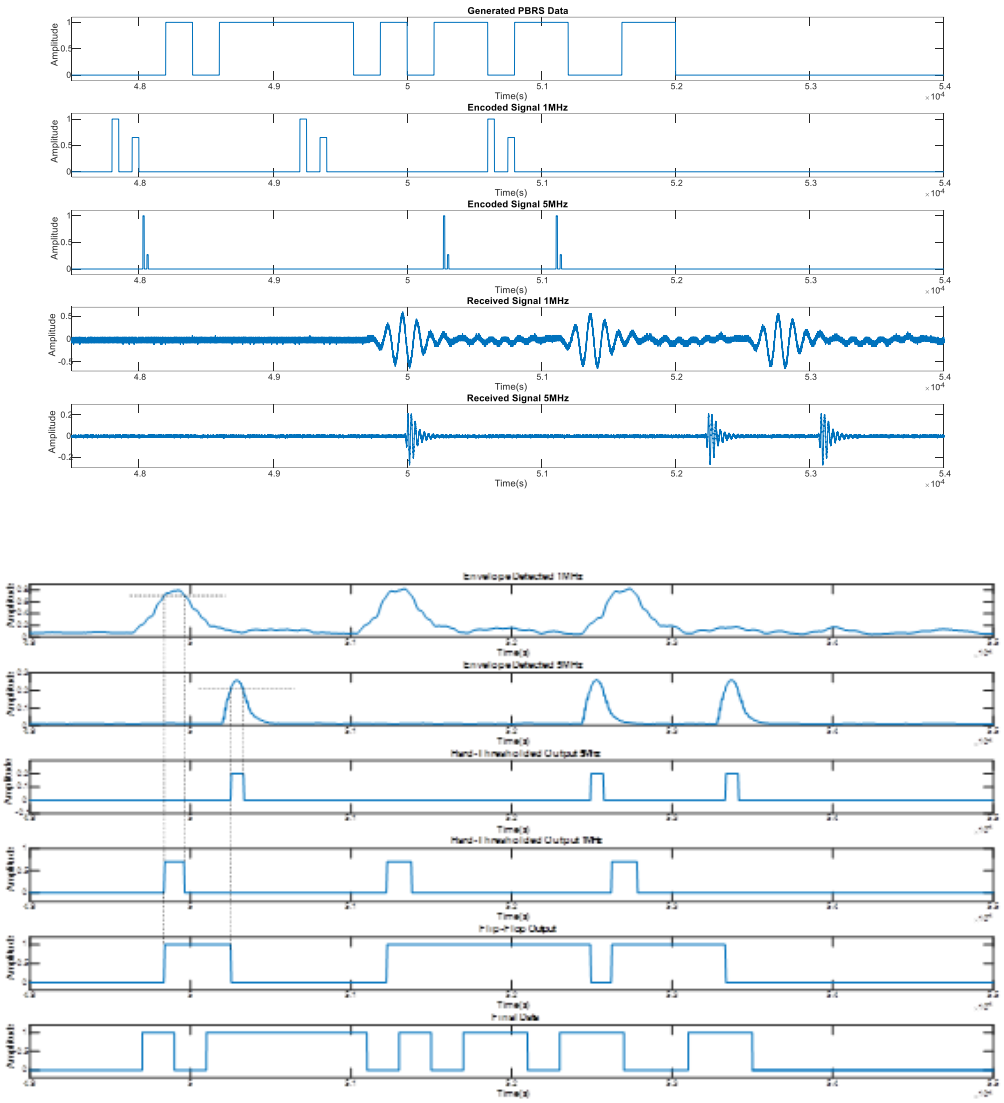


Fig.4.21. A summary of all the stages of INTERIM (From top to bottom): Generated PBRS Data – INTERIM for transducer 1- INTERIM for transducer 2-The received signal from transducer 1- The received signal from transducer 2-The outcome of envelope detection of the 1MHz signal- The outcome of envelope detection of the 5MHz signal- The outcome of hard-thresholding of the 5MHz signal- The outcome of hard-thresholding of the 1MHz signal- The output of the flip-flop – The recovered data

This process was repeated for N=6. The main consideration when choosing the number of bits in a symbol is that by increasing the number of bits in a symbol the error rate decreases; This is since

the noise and other sources of error have the same effect on the symbols but on a larger number of bits. The other consideration is that with a too large number of bits, the bit rate decreases as the symbol time multiplies by 2 with each increase in number of bits.

To conclude, there is a trade-off when choosing the number of bits. According to our experimental results, N = 7 resulted in a bit error rate of less than 2% percent which is the reported threshold in according to the literature. The experiment with N = 6 resulted in an 800-kbps data rate but with a bit error rate of 6% which shows that this work has a huge increase in data rate compared to the similar works. A summary of the results is shown in Table 4.

Table 4 Summary of results

| Number of Bits | Guard Time | Symbol Time | Time Resolution | Bit Rate | Bit Error Rate |
|---|---|---|---|---|---|
| 7 | 0.8 µs | 14 µs | 0.1 µs | 500 kbps | 1.4% |
| 6 | 0.7 µs | 7.5 µs | 0.1 µs | 800 kbps | 6% |

Another important achievement of INTERIM is the improvement over similar works particularly PHM. As mentioned earlier, the simulated tone burst width resulting from EIP complexes are not reflected in experiment. As it can be seen in Fig.4.22, the resulting tone burst widths of the 1 MHz and 5 MHz EIP complexes are 10 µs and 3.2 µs respectively. The measured tone burst widths result in a 100 kbps and 312 kbps data rates whereas in INTERIM a data rate of 800 kbps is achieved using the same transducers.

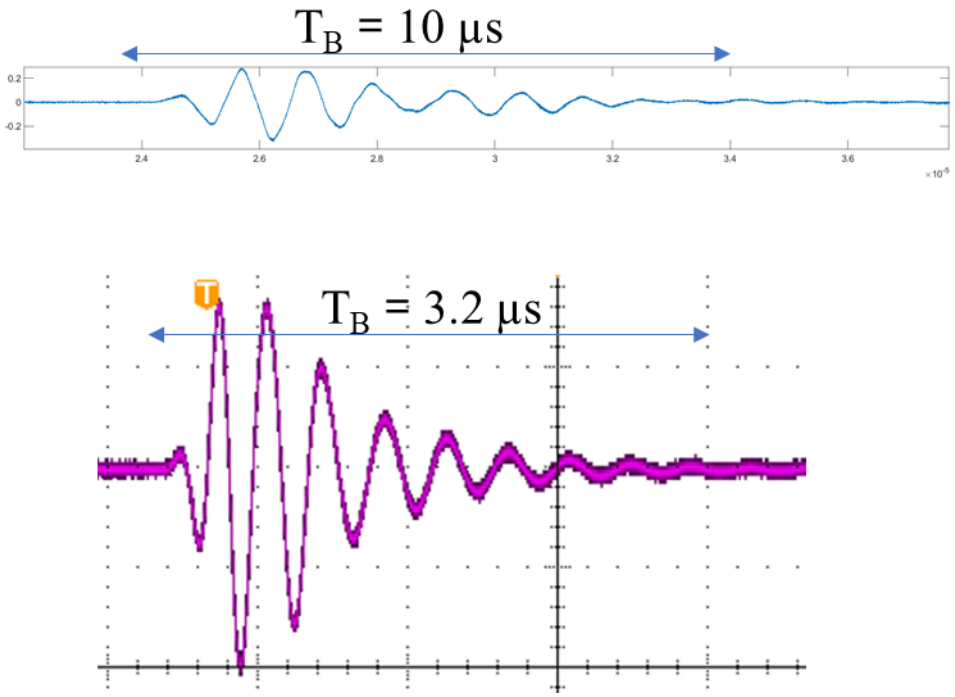


Fig.4.22. Measured tone burst widths corresponding to a 1 MHz (top) and 5 MHz (bottom) EIP complex

## 4.6. Error Analysis

The next step is to characterize the bit error rate (BER) using the signal to noise ratio (SNR). To investigate the BER-SNR relationship, the modulation is evaluated using the same sequence under identical conditions but with varying signal-to-noise ratios, and bit error rate is computed for each of these SNR values.

In general, when dealing with schemes based on width/interval, even a low inaccuracy can result in an inflated bit error rate. Assuming a margin of error as small as 0.1 µs, this slight inaccuracy can result in the perception of a bit sequence of $(0111111)_7 = 63$ as $(1000000)_7 = 64$, which is a seven-bit error induced by a small amount of noise. To better represent the error margin of INTERIM, the difference between the spacings of the original and recovered signals, divided by the time step is used. As predicted, the bit error rate decreases when the signal to noise ratio

increases as shown in Fig.4.23. This is because as the signal becomes more significant compared to noise, the demodulation becomes less error-prone.

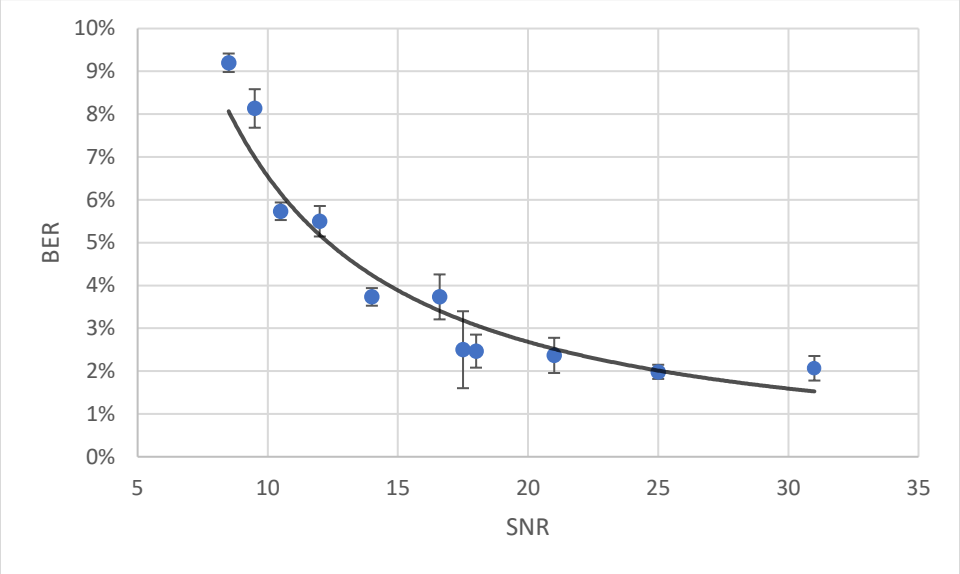


Fig.4.23. The bit error rate (BER) in relationship to signal-to-noise (SNR) ratio with error bars representing standard deviation

Another component of demodulation that can result in an error is the hard-threshold cut-off voltage. The cut-off voltage used to determine whether a received signal is interpreted as "0" or "1" can introduce errors by altering the spacing between the two set and reset pulses. When the threshold voltage gets closer to the peak voltage of the signal, the noise contribution diminishes resulting in a less error, as demonstrated in Fig.4.24.

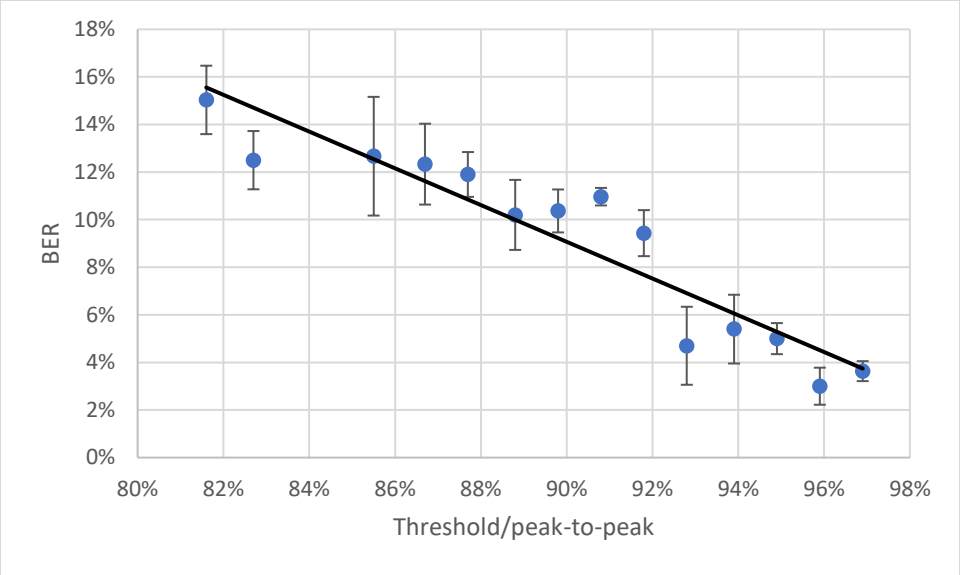


Fig.4.24. Bit error rate (BER) increases as the threshold level decreases in relation to the output peak-to-peak with error bars representing standard deviation

# Chapter 5: Conclusion and future steps

# Chapter 5: Conclusion and Future Direction

As a conclusion, this thesis reports a novel modulation scheme that has the potential to significantly raise the maximum data rates achieved in earlier studies of ultrasonic data telemetry and opens a wide range of opportunities for future development. The proposed technique, called INTERIM, uses the spacing between the excitation of two transmitting transducers with different central frequencies to transmit a randomly generated signal. By using the spacing of two transducers rather than the transient nature of one transducer, this scheme tackles the limit posed by the small operating frequencies of ultrasonic transmission.

The fact that the bit error rate remains reasonably low gives this work a considerable advancement in comparison to previous schemes. Also, the consumed power to transmit each bit is decreased compared to the similar works since INTERIM sends two pulse complexes for each symbol rather than each bit. Furthermore, the implementation of INTERIM is relatively simple since only common and known blocks such as flip-flops and band-pass filters are used. Table 5 summarises the performance of the INTERIM technique and compares it with the existing literature.

Table 5 Performance Comparison

| | This work | [49] (2020) | [2] (2018) | [33] (2017) | [48] (2016) |
|---|---|---|---|---|---|

| **Modulation Technique** | INTERIM | PPM | Pulse Harmonic Modulation | QPSK | OOK/ASK |
|---|---|---|---|---|---|
| **Transducers** | 2 Pairs | 1 Pair | 1 Pair | 2 Pairs | 1 Pair |
| **Carrier Frequency** | 1 MHz & 5 MHz | 0.7 MHz | 1 MHz | 1 MHz | 1 MHz |
| **Data Rate** | 500-800 kbps | 180 kbps | 350 kbps | 250 kbps | 50 kbps |
| **Distance between Tx and Rx** | 5 cm | 12 cm | 3 cm | 5 cm | N/A |
| **Medium** | Water | Phantom | N/A | Mineral Oil | N/A |
| **Results** | Experiment | Experiment | Simulation | Experiment | Experiment |
| **BER** | 1.4% | $10^{-6}$ | 2% | $10^{-4}$ | N/A |

A drawback of this technique is the additional power and circuitry needed to support two sets of transducers. This limitation is a small price to pay because the power limitation set by FDA for ultrasonic telemetry is much higher than electromagnetic telemetry; thus, the increased power used in this work is not of concern in terms of damaging human body tissue.

Considering all that has been reported and accomplished, the area of ultrasonic data telemetry is still in its infancy and has enormous potential for expansion. As mentioned in the first chapter of this study, the data rate used in this area is still in the hundreds of kilobits per second range, which needs be increased to broaden the use of ultrasonic data telemetry.

According to the existing literature, most notable works are constrained by the ultrasonic telemetry's limited operating frequency. The primary contribution and innovation of INTERIM is

that it overcomes this constraint and enables data rates to reach the Mbps range, allowing utilization of the INTERIM in a larger range of applications such as image processing.

The next step for INTERIM is the move towards implantability. ASIC implementation of the transmitter and receiver circuitry is a major step as the implant size needs to be in the millimeter-range for placement in the body. Another possible way to move toward implantability could be using custom-made transducers. The transducers utilized in this project are packaged transducers and too large for implantation. As a result, a 3D printing of the employed transducers would facilitate the implantability of INTERIM. Also, the flexibility provided by INTERIM and using two temporally-spaced excitations can be combined with other methods to further improve the data rate in existing literature.

# References


[1] K. Keramatzadeh and A. M. Sodagar, "Design and implementation of an ultrasonic link for concurrent telemetry of multiple data streams to implantable biomedical microsystems," in *2018 IEEE 61st International Midwest Symposium on Circuits and Systems (MWSCAS)*, 2018, pp. 1090–1093.

[2] K. Keramatzadeh and A. M. Sodagar, "High-rate ultrasonic link for data telemetry to implantable biomedical microsystems using pulse excitation," in *2018 IEEE Life Sciences Conference (LSC)*, 2018, pp. 17–20.

[3] L. E. Kinsler, A. R. Frey, A. B. Coppens, and J. v Sanders, "The acoustic wave equation and simple solutions," *Fundamentals of acoustics. Hoboken: Wiley*, pp. 113–148, 2000.

[4] G. S. Kino, *Acoustic Waves: Devices, Imaging, and Analog Signal Processing (Prentice-Hall Signal Processing Series)*. Prentice Hall, 1987.

[5] S. Ozeri and D. Shmilovitz, "Ultrasonic transcutaneous energy transfer for powering implanted devices," *Ultrasonics*, vol. 50, no. 6, pp. 556–566, 2010.

[6] D. T. Blackstock, "Fundamentals of physical acoustics." Acoustical Society of America, 2001.

[7] P. N. T. Wells, *Biomedical ultrasonics*. Academic press, 1977.

[8] F. A. Duck, A. C. Baker, and H. C. Starritt, *Ultrasound in medicine*. CRC Press, 2020.

[9] S. Ozeri, D. Shmilovitz, S. Singer, and L. Martinez-Salamero, "The mathematical foundation of distributed interleaved systems," *IEEE Transactions on Circuits and Systems I: Regular Papers*, vol. 54, no. 3, pp. 610–619, 2007.

[10] A. Arnau, *Piezoelectric transducers and applications*, vol. 2004. Springer, 2004.

[11] P. R. Hoskins, A. Thrush, K. Martin, and T. A. Whittingham, "Diagnostic ultrasound physics and equipment, Greenwich Med." Media, 2003.

[12] I. F. Akyildiz, D. Pompili, and T. Melodia, "Underwater acoustic sensor networks: research challenges," *Ad hoc networks*, vol. 3, no. 3, pp. 257–279, 2005.

[13] R. J. Urick, "Principles of Underwater Sound, McGraw-hill," *New York*, 1983.

[14] T. C. Chang, M. Wang, and A. Arbabian, "Multi-access networking with wireless ultrasound-powered implants," in *2019 IEEE Biomedical Circuits and Systems Conference (BioCAS)*, 2019, pp. 1–4.

[15] B. Jaafar, J. Neasham, G. Chester, and P. Degenaar, "Ultrasonic wireless powering link of visual cortical prosthesis implant," in *2017 IEEE Biomedical Circuits and Systems Conference (BioCAS)*, 2017, pp. 1–4.

[16] M. Meng and M. Kiani, "Gastric seed: Toward distributed ultrasonically interrogated millimeter-sized implants for large-scale gastric electrical-wave recording," *IEEE Transactions on Circuits and Systems II: Express Briefs*, vol. 66, no. 5, pp. 783–787, 2019.

[17] A. Rashidi, S. Hosseini, K. Laursen, and F. Moradi, "STARDUST: Optogenetics, Electrophysiology and Pharmacology with an Ultrasonically Powered DUST for Parkinson's Disease," in *2019 26th IEEE International Conference on Electronics, Circuits and Systems (ICECS)*, 2019, pp. 109–110.

[18] G. E. Santagati and T. Melodia, “Experimental evaluation of impulsive ultrasonic intra-body communications for implantable biomedical devices,” *IEEE Transactions on Mobile Computing*, vol. 16, no. 2, pp. 367–380, 2016.
[19] A. Arbabian *et al.*, “Sound technologies, sound bodies: Medical implants with ultrasonic links,” *IEEE Microwave Magazine*, vol. 17, no. 12, pp. 39–54, 2016.
[20] Olympus Corporation, “Generating Ultrasound (Transducers).”
[21] R. Krimholtz, D. A. Leedom, and G. L. Matthaei, “New equivalent circuits for elementary piezoelectric transducers,” *Electronics Letters*, vol. 6, no. 13, pp. 398–399, 1970.
[22] W. P. Mason, *Electromechanical transducers and wave filters*. D. Van Nostrand Company, 1948.
[23] W. P. Mason, *Physical acoustics and the properties of solids*. van Nostrand, 1958.
[24] M. Redwood, “Transient performance of a piezoelectric transducer,” *The journal of the acoustical society of America*, vol. 33, no. 4, pp. 527–536, 1961.
[25] U.S. Department of Health and Human Services Food and Drug Administration Center for Devices and Radiological Health, *Marketing Clearance of Diagnostic Ultrasound Systems and Transducers*. 2019.
[26] F. W. Kremkau, “IEEE Guide for Medical Ultrasound Field Parameter Measurements,” *New York, Institute of Electrical and Electronics Engineers*, 1990.
[27] S. A. W. D. Subcommittee, “IEEE Standard Terms and Definitions for Surface Acoustic Wave (SAW) Devices,” 1993.
[28] H. S. Gougheri, A. Dangi, S.-R. Kothapalli, and M. Kiani, “A comprehensive study of ultrasound transducer characteristics in microscopic ultrasound neuromodulation,” *IEEE Trans Biomed Circuits Syst*, vol. 13, no. 5, pp. 835–847, 2019.
[29] J.-Y. Tsai, K.-H. Huang, J.-R. Wang, S.-I. Liu, and P.-C. Li, “Ultrasonic wireless power and data communication for neural stimulation,” in *2011 IEEE International Ultrasonics Symposium*, 2011, pp. 1052–1055.
[30] J. Zhou, A. Kim, M. Ochoa, H. Jiang, and B. Ziaie, “An ultrasonically powered micropump for on-demand in-situ drug delivery,” in *2016 IEEE 29th International Conference on Micro Electromechanical Systems (MEMS)*, 2016, pp. 349–352.
[31] T. Maleki, N. Cao, S. H. Song, C. Kao, S.-C. Ko, and B. Ziaie, “An ultrasonically powered implantable micro-oxygen generator (IMOG),” *IEEE transactions on Biomedical Engineering*, vol. 58, no. 11, pp. 3104–3111, 2011.
[32] S. H. Song, A. Kim, and B. Ziaie, “Omnidirectional ultrasonic powering for millimeter-scale implantable devices,” *IEEE Transactions on Biomedical Engineering*, vol. 62, no. 11, pp. 2717–2723, 2015.
[33] M. L. Wang and A. Arbabian, “Exploiting spatial degrees of freedom for high data rate ultrasound communication with implantable devices,” *Applied Physics Letters*, vol. 111, no. 13, p. 133503, 2017.
[34] M. Meng and M. Kiani, “A hybrid inductive-ultrasonic link for wireless power transmission to millimeter-sized biomedical implants,” *IEEE Transactions on Circuits and Systems II: Express Briefs*, vol. 64, no. 10, pp. 1137–1141, 2016.
[35] Y.-S. Luo *et al.*, “Ultrasonic power/data telemetry and neural stimulator with OOK-PM signaling,” *IEEE Transactions on Circuits and Systems II: Express Briefs*, vol. 60, no. 12, pp. 827–831, 2013.

[36] F. Mazzilli, C. Lafon, and C. Dehollain, “A 10.5 cm ultrasound link for deep implanted medical devices,” *IEEE Trans Biomed Circuits Syst*, vol. 8, no. 5, pp. 738–750, 2014.
[37] A. Rashidi, K. Laursen, S. Hosseini, and F. Moradi, “An ultrasonically powered optogenetic microstimulators with power-efficient active rectifier and charge reuse capability,” in *2019 IEEE International Symposium on Circuits and Systems (ISCAS)*, 2019, pp. 1–5.
[38] A. Rashidi, K. Laursen, S. Hosseini, and F. Moradi, “Overvoltage protection circuits for ultrasonically powered implantable microsystems,” in *2019 41st Annual International Conference of the IEEE Engineering in Medicine and Biology Society (EMBC)*, 2019, pp. 4354–4358.
[39] F. Mazzilli, E. G. Kilinc, and C. Dehollain, “3.2 mW ultrasonic LSK modulator for uplink communication in deep implanted medical devices,” in *2014 IEEE Biomedical Circuits and Systems Conference (BioCAS) Proceedings*, 2014, pp. 636–639.
[40] T. C. Chang, M. L. Wang, J. Charthad, M. J. Weber, and A. Arbabian, “27.7 A 30.5 mm 3 fully packaged implantable device with duplex ultrasonic data and power links achieving 95kb/s with< 10− 4 BER at 8.5 cm depth,” in *2017 IEEE International Solid-State Circuits Conference (ISSCC)*, 2017, pp. 460–461.
[41] J. Zhou, A. Kim, and B. Ziaie, “An ultrasonically controlled power management system for implantable biomedical devices,” in *2015 IEEE Biomedical Circuits and Systems Conference (BioCAS)*, 2015, pp. 1–4.
[42] J. Charthad, M. J. Weber, T. C. Chang, and A. Arbabian, “A mm-sized implantable medical device (IMD) with ultrasonic power transfer and a hybrid bi-directional data link,” *IEEE Journal of solid-state circuits*, vol. 50, no. 8, pp. 1741–1753, 2015.
[43] M. Meng and M. Kiani, “Design and optimization of ultrasonic wireless power transmission links for millimeter-sized biomedical implants,” *IEEE Trans Biomed Circuits Syst*, vol. 11, no. 1, pp. 98–107, 2016.
[44] S. Hosseini, K. Laursen, A. Rashidi, and F. Moradi, “Multi-ring ultrasonic transducer on a single piezoelectric disk for powering biomedical implants,” in *2019 41st Annual International Conference of the IEEE Engineering in Medicine and Biology Society (EMBC)*, 2019, pp. 3827–3830.
[45] M. L. Wang, T. C. Chang, and A. Arbabian, “Ultrasonic implant localization for wireless power transfer: Active uplink and harmonic backscatter,” in *2019 IEEE International Ultrasonics Symposium (IUS)*, 2019, pp. 818–821.
[46] S. Haykin and M. Moher, *Introduction to analog and digital communications*. New York, NY: Wiley, 2007.
[47] Amir M. Sodagar, “Implentable Biomedical Microsystems.” York University, Toronto, 2019.
[48] F. Mazzilli and C. Dehollain, “184 μW ultrasonic on–off keying/amplitude-shift keying demodulator for downlink communication in deep implanted medical devices,” *Electronics Letters*, vol. 52, no. 7, pp. 502–504, 2016.
[49] G. E. Santagati and T. Melodia, “An implantable low-power ultrasonic platform for the Internet of Medical Things,” in *IEEE INFOCOM 2017-IEEE Conference on Computer Communications*, 2017, pp. 1–9.

[50] T. Bos, W. Dehaene, and M. Verhelst, “Ultrasound in-body communication with OFDM through multipath realistic channels,” in *2019 IEEE Biomedical Circuits and Systems Conference (BioCAS)*, 2019, pp. 1–4.
[51] R. Rogalin and M. Srinivasan, “Maximum likelihood synchronization for pulse position modulation with inter-symbol guard times,” in *2016 IEEE Global Communications Conference (GLOBECOM)*, 2016, pp. 1–6.
[52] K. J. Quirk, J. W. Gin, and M. Srinivasan, “Optical PPM synchronization for photon counting receivers,” in *MILCOM 2008-2008 IEEE Military Communications Conference*, 2008, pp. 1–7.